

ALPHA-MODELING STRATEGY FOR LES OF TURBULENT MIXING

Bernard J. Geurts

*Faculty of Mathematical Sciences, University of Twente, P.O. Box 217,
7500 AE Enschede, The Netherlands*

b.j.geurts@math.utwente.nl

Darryl D. Holm

Theoretical Division and Center for Nonlinear Studies, Los Alamos National Laboratory, MS B284 Los Alamos, NM 87545, USA

dholm@lanl.gov

Abstract The α -modeling strategy is followed to derive a new subgrid parameterization of the turbulent stress tensor in large-eddy simulation (LES). The LES- α modeling yields an explicitly filtered subgrid parameterization which contains the filtered nonlinear gradient model as well as a model which represents ‘Leray-regularization’. The LES- α model is compared with similarity and eddy-viscosity models that also use the dynamic procedure. Numerical simulations of a turbulent mixing layer are performed using both a second order, and a fourth order accurate finite volume discretization. The Leray model emerges as the most accurate, robust and computationally efficient among the three LES- α subgrid parameterizations for the turbulent mixing layer. The evolution of the resolved kinetic energy is analyzed and the various subgrid-model contributions to it are identified. By comparing LES- α at different subgrid resolutions, an impression of finite volume discretization error dynamics is obtained.

Keywords: large-eddy simulation, dispersion, dissipation, similarity, numerical error dynamics

1. Introduction

Accurate modeling and simulation of turbulent flow is a topic of intense ongoing research. The approaches to this problem area can be distinguished, e.g., by the amount of detail that is intended to be included in the physical and numerical description. Simulation strategies

that aim to calculate the full, unsteady solution of the governing Navier-Stokes equations are known as direct numerical simulations (DNS). The DNS approach does not involve any modeling or approximation except its numerical nature and in principle it can provide solutions that possess all dynamically relevant flow features [1, 2]. In turbulent flow, these features range from large, geometry dependent scales to very much smaller dissipative length-scales. While accurate in principle, the DNS approach is severely restricted by limitations in spatial and temporal resolution, even with modern computational capabilities, because of the tendency of fluid flow to cascade its energy to smaller and smaller scales.

This situation summons alternative, restricted simulation approaches to the turbulent flow problem that are aimed at capturing the primary features of the flow above a certain length-scale only. A prominent example of this is the large-eddy simulation (LES) strategy [3]. Rather than aiming for a precise and complete numerical treatment of all features that play a role in the evolution of the flow, an element of turbulence modeling is involved in LES [4]. In the filtering approach to LES, this modeling element is introduced by applying a spatially localized filter operation to the Navier-Stokes equations [5]. This introduces a smoothing of the flow features and a corresponding reduction in the flow complexity [6]. One commonly adopts spatial convolution filters which effectively remove the small-scale flow features that fall below an externally introduced length-scale Δ , referred to as the filter-width. This smoothing can significantly reduce the requirements on the resolution and, thus, allow LES to be performed for much more realistic situations than DNS, e.g., at higher Reynolds number, within the same computational capabilities [7]. This constitutes the main virtue of LES.

The LES approach is conceptually different from the Reynolds Averaged Navier-Stokes (or, RANS) approach, which is based on statistical arguments and exact ensemble averages that raise the classic turbulence closure problem. When the spatially localized smoothing operation in LES is applied to the nonlinear convective terms in the Navier-Stokes equations, this also gives rise to a closure problem that needs to be resolved. Thus, the LES approach must face its own turbulence closure problem: How to model the effects of the filtered-out scales in terms of the remaining resolved fields?

In the absence of a comprehensive theory of turbulence, empirical knowledge about subgrid-scale modeling is essential but still incomplete. Since in LES only the dynamical effects of the smaller scales need to be represented, the modeling is supposed to be simpler and more straightforward, compared to the setting encountered in statistical modeling such as in RANS. To guide the construction of suitable models we ad-

vocate the use of constraints based on rigorous properties of the LES modeling problem such as realizability conditions [8] and algebraic identities [5, 6]. A thoughtful overview of these constraints is given in [9].

In this paper, we follow the α -modeling approach to the LES closure problem. The α -modeling approach is based on the Lagrangian-averaged Navier-Stokes- α equations (LANS- α , or NS- α) described below. The LANS- α approach eliminates some of the heuristic elements that would otherwise be involved in the modeling. The original LANS- α theory also involves an elliptic operator inversion in defining its stress tensor. When we apply filtering in defining the LANS- α stress tensor, instead of the operator inversion in the original theory, we call it LES- α .

Background and references for LANS- α , or NS- α equations.

The inviscid LANS- α equations (called Euler- α , in the absence of viscosity) were introduced through a variational formulation in [10], [11] as a generalization to 3D of the integrable inviscid 1D Camassa-Holm equation discovered in [12]. A connection between turbulence and the solutions of the viscous 3D Camassa-Holm, or Navier-Stokes-alpha (NS- α) equations was identified, when viscosity was introduced in [13]–[15]. Specifically, the steady analytical solution of the NS- α equations was found to compare successfully with experimental and numerical data for mean velocity and Reynolds stresses for turbulent flows in pipes and channels over a wide range of Reynolds numbers. These comparisons suggested the NS- α equations could be used as a closure model for the mean effects of subgrid excitations. Numerical tests further substantiating this intuition were performed and reported in [16].

An alternative more “physical” derivation for the inviscid NS- α equations (Euler- α), was introduced in [17] (see also [14]). This alternative derivation was based on substituting in Hamilton’s principle the decomposition of the Lagrangian fluid-parcel trajectory into its mean and fluctuating components at linear order in the fluctuation amplitude. This was followed by making the Taylor hypothesis for frozen-in turbulence and averaging at constant Lagrangian coordinate, before taking variations. Hence, the descriptive name Lagrangian-averaged Navier-Stokes- α equations (LANS- α) was given for the viscous version of this model. A variant of this approach was also elaborated in [18] but this resulted in a second-grade fluid model, instead of the viscous LANS- α equations, because the choice of dissipation made in [18] differed from the Navier-Stokes dissipation chosen in [13]–[17]. The geometry and analysis of the inviscid Euler- α equations was presented in [19], [20]. The analysis of global existence and well-posedness for the viscous LANS- α was given for periodic domains in [21] and was modified for bounded

domains in [22]. For more information and a guide to the previous literature specifically about the $\text{NS}-\alpha$ model, see paper [23]. The latter paper also discusses connections to standard concepts and scaling laws in turbulence modeling, including relationships of the $\text{NS}-\alpha$ model to large eddy simulation (LES) models that are pursued farther in the present paper. Related results interpreting the $\text{NS}-\alpha$ model as an extension of scale similarity LES models of turbulence are also reported in [24]. A numerical comparison of LANS- α model results with LES models for the late stages of decaying homogeneous turbulence is discussed in [25]. Vortex interactions in the early stages of 3D turbulence decay are studied numerically with LANS- α and compared with both DNS and the Smagorinsky eddy viscosity approach in [26].

Three contributions in the present approach. Stated most simply, the LANS- α approach may be interpreted as a closure model for the turbulent stress tensor that is derived from Kelvin's circulation theorem, using a smoothed transport velocity, as discussed in [23], [24], [27]. A new development within this approach is introduced here that gives rise to an explicitly filtered similarity-type model [28] for the turbulent stress tensor, composed of three different contributions. The first contribution is a filtered version of the nonlinear gradient model. The unfiltered version of this model is also known as the 'Clark' model [29, 30], the 'gradient' model [31] or the 'tensor-diffusivity' model [32]. The second contribution, when combined with the filtered nonlinear gradient model, represents the so-called 'Leray regularization' of Navier-Stokes dynamics [33]. Finally, a new third contribution emerges from the derivation which completes the full LES- α model and endows it with its own Kelvin's circulation theorem.

To investigate the physical and numerical properties of the resulting three-part LANS- α subgrid parameterization, we consider a turbulent mixing layer [34]. This flow is well documented in literature and provides a realistic canonical flow problem [35] suitable for testing and comparison with predictions arising from more traditional subgrid model developments [7]. In particular, we consider similarity, and eddy-viscosity modeling, combined with the dynamic procedure based on Germano's identity [5, 6, 36], to compare with LES- α . In addition to the full LES- α model, in our comparisons we also consider the two models that are contained in it, i.e., the filtered nonlinear gradient model and the Leray model. We will refer to all three as LES- α models. For all these models, the explicit filtering stage is essential. Without this filtering operation in the definition of the models, a finite time instability is observed to arise in the simulations. The basis for this instability can be traced

back to the presence of antidi diffusion in the nonlinear gradient contribution. We sketch an analysis of the one-dimensional Burgers equation, following [31], to illustrate this instability and show, through simulation, that increasing the subgrid resolution further enhances this instability. Analyzing the resolved kinetic energy dynamics reveals that this instability is associated with an excessive contribution to back-scatter.

The ‘nonlinearly dispersive’ filtered models that arise in LES- α are reminiscent of similarity LES models [24]. The LES- α model separates the resolved kinetic energy (RKE) of the flow into the sum of two contributions: namely, the energies due to motions at scales that are either greater, or less than an externally determined length-scale (α). The two contributions are modeled by

$$RKE = RKE^{(>)} + RKE^{(<)} \quad (1)$$

As we shall describe later in reviewing the LES- α strategy, the kinetic energy $RKE^{(<)}$ of turbulent motions at scales less than α is modeled by a term proportional to the *rate of dissipation* of the kinetic energy $RKE^{(>)}$ at scales greater than α . (The time-scale in the proportionality constant is the viscous diffusion time $\alpha^2/2\nu$.)

A key aspect of the LES- α dynamics is the exchange, or conversion, of kinetic energy between $RKE^{(>)}$ and $RKE^{(<)}$. We focus on the contributions to the dynamics of the resolved kinetic energy $RKE^{(>)}$ at scales greater than α that arise from the different terms in the LES- α models. The filtered nonlinear gradient model, the Leray model and the full LES- α model all contribute to the reduction of the $RKE^{(>)}$ in the laminar stages of the flow. This corresponds to forward scatter of $RKE^{(>)}$ into $RKE^{(<)}$ outweighing backward scatter. In the developing turbulent flow regime, the resolved kinetic energy $RKE^{(>)}$ of the full LES- α model may decrease too slowly compared to DNS, and for some settings of the (numerical) parameters can even become reactive in nature, thereby back-scattering too much kinetic energy from $RKE^{(<)}$ into $RKE^{(>)}$. In contrast, the contribution of the Leray model to the $RKE^{(>)}$ dynamics remains forward in nature and appears to settle around some negative, nonzero value in the turbulent regime. All the LES- α models show contributions to both forward and backward scatter of RKE. It is observed that in the full LES- α model two of the three terms almost cancel in the evolution of resolved kinetic energy $RKE^{(>)}$. This cancellation nearly reduces the full LES- α model to the filtered nonlinear gradient model.

The mixing layer simulations indicate that the Leray subgrid model provides more accurate predictions compared to both the filtered nonlinear gradient and the full LES- α model. This is based on comparisons that include mean flow quantities, fluctuating flow properties and the

energy spectrum. In addition, the Leray LES- α model appears more robust with respect to changes in numerical parameters. Predictions based on this model compare quite favorably with those obtained using dynamic (mixed) models and filtered DNS results. The Leray model combines this feature with a strongly reduced computational cost and is favored for this reason, as well. In addition, a number of classic mathematical properties (e.g., existence and uniqueness of strong solutions) can be proven rigorously for fluid flows that are modeled with Leray's regularization. These can be used to guide further developments of this model such as extensions to more complex flows at higher Reynolds number. This is a topic of current research and will be published elsewhere [37].

Apart from the problem of modeling the subgrid-scale stresses, any actual realization of LES is inherently endowed with (strongly) interacting errors arising from the required use of marginal numerical resolution [38, 39, 40, 41]. The accuracy of the predictions depends on the numerical method and subgrid resolution one uses. We consider in some detail numerical contamination of a 'nonlinear gradient fluid' and a 'Leray fluid,' which are defined as the hypothetical fluids governed by the corresponding subgrid model. In this analysis we are consequently not concerned with how accurately the modeled equations represent filtered DNS results. Rather, we focus on the numerical contamination of the predictions. For this purpose we compare two finite volume spatial discretization methods, one at second order, and the other at fourth order accuracy.

The subgrid modeling and the spatial discretization of the equations give rise to a computational dynamical system whose properties are intended to simulate those of the filtered Navier-Stokes equations. The success of this simulation depends of course on the properties of the model, as well as of the spatial discretization method and the subgrid resolution. The model properties are particularly important in view of the marginal subgrid resolution used in present-day LES. We consider the role of the numerical method at various resolutions and various ratios of the filter-width Δ compared to the grid-spacing h . Let Δ be a fixed constant. In cases of large ratios $\Delta/h \gg 1$ one approximates the grid-independent LES solution corresponding to the given value of Δ , and the accuracy of its predictions will be limited by the quality of the assumed subgrid model. At the other extreme, one may assume Δ/h to be rather small and numerical effects can constitute a large source of error. Through a systematic variation of the ratio Δ/h at constant Δ we can identify the contributions of the numerical method at coarse resolutions.

This will give an impression of how the computational dynamical system is affected by variations in the resolution and the numerical method.

The organization of this chapter is as follows. In section 2 we introduce the large-eddy simulation problem and identify the closure problem and some of its properties. The treatment of this closure problem using the α -framework is sketched, together with more conventional subgrid parameterization that involves the introduction of similarity, and eddy-viscosity modeling. Finally, we analyze the instabilities associated with the use of the unfiltered nonlinear gradient model. In section 3 we introduce the numerical methods used and consider the simulation of a turbulent mixing layer. Some direct and large-eddy simulation results will be shown. In section 4 we focus on the LES- α models and consider the dynamics of the resolved kinetic energy in each of the three cases. This comparison provides a framework for understanding how the different LES- α subgrid models function. We proceed with an assessment of the numerical error dynamics at relatively coarse subgrid resolutions. A summary and concluding remarks for the chapter are given in section 5.

2. Large-eddy simulation and α -modeling

This section sketches the traditional approach to large-eddy simulation, which arises from direct spatial filtering of the Navier-Stokes equations (section 2.1). The algebraic and analytic properties of the LES modeling problem will be discussed first. The LES closure problem will then be considered in the α -framework of turbulent flow, derived via Kelvin's circulation theorem for a smoothed, spatially filtered transport velocity (section 2.2). The closure of the filtered fluid flow problem achieved this way will be compared with the more traditional methods of similarity, and eddy-viscosity modeling for LES. The latter is introduced in section 2.3 together with the dynamic procedure based on Germano's identity. We also sketch a stability analysis of the one-dimensional filtered Burgers equation involving the nonlinear gradient subgrid model that illustrates the instabilities associated with this model (section 2.4).

2.1. Spatially filtered fluid dynamics

We consider the incompressible flow problem in d spatial dimensions. The Cartesian velocity fields u_i ($i = 1, \dots, d$) and the normalized pressure field p constitute the complete solution. The velocity field is considered to be solenoidal and the evolution of the solution is described by the Navier-Stokes equations. These are conservation laws for mass and momentum, respectively, that can be written in the absence of forcing

as

$$\partial_j u_j = 0 \quad (2)$$

$$\partial_t u_i + \partial_j (u_i u_j) + \partial_i p - \frac{1}{Re} \partial_{jj} u_i = 0 \quad (3)$$

where ∂_t and ∂_j denote, respectively, partial differential operators in time t and Cartesian coordinate x_j , $j = 1, \dots, d$. The quantity $Re = u_r l_r / \nu_r$ is the Reynolds number based on reference velocity (u_r), reference length (l_r) and reference kinematic viscosity (ν_r), which were selected to non-dimensionalize the governing equations. Repeated indices are summed over their range, except where otherwise noted.

Equations (2 - 3) model incompressible flow in all its spatial and temporal details. In deriving approximate equations that are specialized to capture the generic large-scale flow features only, one applies a spatial filter operation $L : u \rightarrow \bar{u}$ to (2 - 3). For simplicity, we restrict to linear convolution filters:

$$\bar{u}(\mathbf{x}, t) = L(u)(\mathbf{x}, t) = \int_{-\infty}^{\infty} G(\mathbf{x} - \boldsymbol{\xi}) u(\boldsymbol{\xi}, t) d\boldsymbol{\xi} = (G * u)(\mathbf{x}, t) \quad (4)$$

in which the filter-kernel G is normalized, i.e., $L(c) = c$ for any constant solution $u = c$. We assume that the filter-kernel G is localized as a function of $\mathbf{x} - \boldsymbol{\xi}$ and a filter-width Δ can be assigned to it. Typical filters which are commonly considered in LES are the top-hat, the Gaussian and the spectral cut-off filter. Here, we restrict ourselves to the top-hat filter which has a filter-kernel given by

$$G(\mathbf{z}) = \begin{cases} \Delta^{-3} & \text{if } |z_i| < \Delta_i/2 \\ 0 & \text{otherwise} \end{cases} \quad (5)$$

where Δ_i denotes the filter-width in the x_i direction and the total filter-width Δ is specified by

$$\Delta^3 = \Delta_1 \Delta_2 \Delta_3 \quad (6)$$

Apart from the filter-kernel in physical space, the Fourier-transform of $G(\mathbf{z})$, denoted by $H(\mathbf{k})$, is important, e.g., for the interpretation of the effect of the filter-operation on signals which are composed of various length-scales. The Fourier-transform of the top-hat filter is given by (no sum in $\Delta_i k_i$)

$$H(\mathbf{k}) = \prod_{i=1}^3 \frac{\sin(\Delta_i k_i / 2)}{\Delta_i k_i / 2} \quad (7)$$

If we consider a general Fourier-representation of a solution $u(\mathbf{x}, t)$,

$$u(\mathbf{x}, t) = \sum_{\mathbf{k}} c_{\mathbf{k}}(t) e^{i\mathbf{k} \cdot \mathbf{x}} \quad (8)$$

the filtered solution can directly be written as

$$\bar{u}(\mathbf{x}, t) = \sum_{\mathbf{k}} (H(\mathbf{k}) c_{\mathbf{k}}(t)) e^{i\mathbf{k} \cdot \mathbf{x}} \quad (9)$$

We notice that each Fourier-coefficient $c_{\mathbf{k}}(t)$ is attenuated by a factor $H(\mathbf{k})$. The normalization condition of the filter-operation implies $H(\mathbf{0}) = 1$. For small values of $|\Delta_i k_i|$ one infers from a Taylor expansion

$$H(\mathbf{k}) = 1 - (1/24) \left((k_1 \Delta_1)^2 + (k_2 \Delta_2)^2 + (k_3 \Delta_3)^2 \right) + \dots \quad (10)$$

which shows the small attenuation of flow features which are considerably larger than the filter-width Δ , i.e., $|\Delta_i k_i| \ll 1$ for $i = 1, 2, 3$. As $|\mathbf{k}|$ increases $H(\mathbf{k})$ becomes smaller while oscillating as a function of $\Delta_i k_i$. Consequently, the coefficients $c_{\mathbf{k}}(t)$ are strongly reduced as $|\Delta_i k_i| \gg 1$ and the small scale features in the solution are effectively taken out by the filter operation. Similarly, the Gaussian filter can be shown to have the same expansion for small $|\Delta_i k_i|$ and reduces to zero monotonously as $|\Delta_i k_i|$ becomes large.

The filter operation L is a convolution integral. Hence, it is a linear operation that commutes with partial derivatives [42, 43]. This property facilitates the application of the filter to the governing equations (2 - 3). A straightforward application of such filters leads to

$$\partial_j \bar{u}_j = 0 \quad (11)$$

$$\partial_t \bar{u}_i + \partial_j (\bar{u}_i \bar{u}_j) + \partial_i \bar{p} - \frac{1}{Re} \partial_{jj} \bar{u}_i = -\partial_j \tau_{ij} \quad (12)$$

where we introduced the turbulent stress tensor

$$\tau_{ij} = \bar{u}_i \bar{u}_j - \bar{u}_i \bar{u}_j \quad (13)$$

We observe that the filtered solution $\{\bar{u}_i, \bar{p}\}$ represents an incompressible flow ($\partial_j \bar{u}_j = 0$). The same differential operator as in (3) acts on $\{\bar{u}_i, \bar{p}\}$ and due to the filtering a non-zero right-hand side has arisen which contains the divergence of the turbulent stress tensor τ_{ij} . This latter term is the so-called subgrid term, and expressing it in terms of the filtered velocity and its derivatives constitutes the closure problem in large-eddy simulation.

The LES modeling problem as expressed above has a number of important, rigorous properties which may serve as guidelines for specifying appropriate subgrid-models for τ_{ij} . In particular, we will briefly review realizability conditions, algebraic identities and transformation properties. Adhering to these basic features of τ_{ij} limits some of the heuristic elements in the subgrid-modeling.

Realizability. It is well known that the Reynolds stress $\overline{u'_i u'_j}$ in RANS is positive semi-definite [44, 45] and the following inequalities hold [46]

$$\tau_{ii} \geq 0 \quad \text{for } i \in \{1, 2, 3\} \quad (\text{no sum}) \quad (14)$$

$$|\tau_{ij}| \leq \sqrt{\tau_{ii} \tau_{jj}} \quad \text{for } i, j \in \{1, 2, 3\} \quad (\text{no sum}) \quad (15)$$

$$\det(\tau_{ij}) \geq 0 \quad (16)$$

If the filtering approach is followed, in general $\tau_{ij} \neq \overline{u'_i u'_j}$ and, therefore, it is relevant to know the conditions under which τ_{ij} is positive semi-definite. Following Vreman *et al.* [8], it can be proved that τ_{ij} in LES is positive semi-definite if and only if the filter kernel $G(\mathbf{x}, \boldsymbol{\xi})$ is positive for all \mathbf{x} and $\boldsymbol{\xi}$. If we assume $G \geq 0$, the expression

$$(f, g) = \int_{\Omega} G(\mathbf{x}, \boldsymbol{\xi}) f(\boldsymbol{\xi}) g(\boldsymbol{\xi}) d\boldsymbol{\xi} \quad (17)$$

defines an inner product and we can rewrite the turbulent stress tensor as:

$$\tau_{ij}(\mathbf{x}) = \int_{\Omega} G(\mathbf{x}, \boldsymbol{\xi}) (u_i(\boldsymbol{\xi}) - \overline{u}_i(\mathbf{x})) (u_j(\boldsymbol{\xi}) - \overline{u}_j(\mathbf{x})) d\boldsymbol{\xi} = (v_i^{\mathbf{x}}, v_j^{\mathbf{x}}) \quad (18)$$

with $v_i^{\mathbf{x}}(\boldsymbol{\xi}) \equiv u_i(\boldsymbol{\xi}) - \overline{u}_i(\mathbf{x})$. In this way the tensor τ_{ij} forms a 3×3 Grammian matrix of inner products. Such a matrix is always positive semi-definite and consequently τ_{ij} satisfies the realizability conditions. The reverse statement can likewise be established, showing that the condition $G \geq 0$ is both necessary and sufficient.

One prefers the turbulent stress tensor τ_{ij} in LES to be realizable for a number of reasons. For example, if τ_{ij} is realizable, the generalized turbulent kinetic energy $k = \tau_{ii}/2$ is a positive quantity. This quantity is required to be positive in subgrid models which involve the k -equation [47]. Several further benefits of realizability and positive filters can be identified [8]; here we restrict to adding that the kinetic energy of \overline{u} is bounded by that of u for positive filter-kernels:

$$\frac{1}{2} \int_{\Omega} |\overline{u}|^2 d\mathbf{x} \leq \frac{1}{2} \int_{\Omega} |u|^2 d\mathbf{x} \quad (19)$$

Requiring realizability places some restrictions on subgrid models. For example, if $G \geq 0$ models for τ should be realizable. Consider, e.g., an eddy-viscosity model m_{ij} given by

$$m_{ij} = -\nu_e \sigma_{ij} + \frac{2}{3} k \delta_{ij} \quad (20)$$

In order for this model to be realizable, a lower bound for k in terms of the eddy-viscosity ν_e arises, i.e., $k \geq \frac{1}{2} \sqrt{3\sigma} \nu_e$ where $\sigma = \frac{1}{2} \sigma_{ij} \sigma_{ij}$ and σ_{ij} is the rate of strain tensor given by $\sigma_{ij} = \partial_i u_j + \partial_j u_i$.

Algebraic identities. The introduction of the product operator $S(u_i, u_j) = u_i u_j$ allows to write the turbulent stress tensor as [6]:

$$\tau_{ij}^L = \overline{u_i u_j} - \overline{u_i} \overline{u_j} = L(S(u_i, u_j)) - S(L(u_i), L(u_j)) = [L, S](u_i, u_j) \quad (21)$$

in terms of the central commutator $[L, S]$ of the filter L and the product operator S . This commutator shares a number of properties with the Poisson-bracket in classical mechanics. Leibniz' rule of Poisson-brackets is in the context of LES known as Germano's identity [5]

$$[\mathcal{L}_1 \mathcal{L}_2, S] = [\mathcal{L}_1, S] \mathcal{L}_2 + \mathcal{L}_1 [\mathcal{L}_2, S] \quad (22)$$

This can also be written as

$$\tau^{\mathcal{L}_1 \mathcal{L}_2} = \tau^{\mathcal{L}_1} \mathcal{L}_2 + \mathcal{L}_1 \tau^{\mathcal{L}_2} \quad (23)$$

and expresses the relation between the turbulent stress tensor corresponding to different filter-levels. In these identities, \mathcal{L}_1 and \mathcal{L}_2 denote any two filter operators and $\tau^K = [K, S]$. The first term on the right-hand side of (23) is interpreted as the 'resolved' term which in an LES can be evaluated without further approximation. The other two terms require modeling of τ at the corresponding filter-levels.

Similarly, Jacobi's identity holds for S , \mathcal{L}_1 and \mathcal{L}_2 :

$$[\mathcal{L}_1, [\mathcal{L}_2, S]] + [\mathcal{L}_2, [S, \mathcal{L}_1]] = -[S, [\mathcal{L}_1, \mathcal{L}_2]] \quad (24)$$

The expressions in (22) and (24) provide relations between the turbulent stress tensor corresponding to different filters and these can be used to dynamically model τ^L . The success of models incorporating Germano's identity (22) is by now well established in applications for many different flows. In the traditional formulation one selects $\mathcal{L}_1 = \mathcal{H}$ and $\mathcal{L}_2 = L$ where \mathcal{H} is the so called test-filter. In this case one can specify Germano's identity [5] as

$$\tau^{\mathcal{H}L}(u) = \tau^{\mathcal{H}}(L(u)) + \mathcal{H}(\tau^L(u)) \quad (25)$$

The first term on the right hand side involves the operator $\tau^{\mathcal{H}}$ acting on the resolved LES field $L(u)$ and during an LES this is known explicitly. The remaining terms need to be replaced by a model. In the dynamic modeling [36] the next step is to assume a base-model m^K corresponding to filter-level K and optimize any coefficients in it, e.g., in a least squares sense [48]. The operator formulation can be extended to include approximate inversion defined by $\mathcal{L}^{-1}(L(x^k)) = x^k$ for $0 \leq k \leq N$ [49]. Dynamic inverse models have been applied in mixing layers [50].

Transformation properties. The turbulent stress tensor τ_{ij} can be shown to be invariant with respect to Galilean transformations. This property also holds for the divergence, i.e., $\partial_j \tau_{ij}$, referred to as the subgrid scale force. Hence, the filtered Navier-Stokes dynamics is Galilean invariant. Suitable subgrid models should at least maintain the Galilean invariance of the divergence of the model, i.e., $\partial_j m_{ij}$. In fact, most subgrid models are represented by tensors which are Galilean invariant. Examples of non-symmetric tensor models have been reported in [24] for which, however, $\partial_j m_{ij}$ was verified to be Galilean invariant.

Likewise, it is of interest to consider a transformation of the subgrid scale stress tensor to a frame of reference rotating with a uniform angular velocity. The full subgrid scale stress tensor transforms in such a way that the subgrid scale force is the same in an inertial and in a rotating frame. Horiuti [51] has recently analyzed several subgrid scale models and showed that some of them do not satisfy this condition. This is an example of how transformation properties of the exact turbulent stress tensor can be used to guide propositions for subgrid modeling.

After closing the filtered equations (11-12) by a subgrid model stress tensor m_{ij} we arrive at the modeled filtered dynamics described in the absence of forcing by

$$\partial_j v_j = 0 \quad (26)$$

$$\partial_t v_i + \partial_j(v_i v_j) + \partial_i P - \frac{1}{Re} \partial_{jj} v_i = -\partial_j m_{ij} \quad (27)$$

whose solution is denoted as $\{v_i, P\}$. Ideally, if m_{ij} and the numerical treatment were correct and had no undesirable effects on the dynamics, one might expect $v_i = \bar{u}_i$. In view of possible sensitive dependence of an actual solution, e.g., on the initial condition, one should not expect instantaneous and point-wise equality of v_i and \bar{u}_i but rather one should expect statistical properties of the filtered and modeled solution to be equal. Assessing the extent to which the properties of $\{v_i, P\}$ and $\{\bar{u}_i, \bar{p}\}$ are correlated allows an evaluation of the quality of the subgrid model, the dynamic effects arising from the numerical method and the interactions between modeling and numerics. In what follows, we will use the notation $\{v_i, P\}$ to distinguish the solution of the subgrid model from the filtered solution $\{\bar{u}_i, \bar{p}\}$.

2.2. Subgrid model derived from Kelvin's theorem

The LES- α modeling scheme we shall use here is based on the well-known viscous Camassa-Holm equations, or LANS- α model. This mod-

eling strategy imposes a ‘cost’ in resolved kinetic energy (RKE) for creation of smaller and smaller excitations below a certain, externally specified length scale, denoted by α . This cost in converting $RKE^{(>)}$ to $RKE^{(<)}$ implies a nonlinear modification of the Navier-Stokes equations which is reactive, or dispersive, in nature instead of being diffusive, as is more common in present-day LES modeling. The modification appears in the nonlinear convection term and can be rewritten in terms of a subgrid model for the turbulent stress tensor. In the LANS- α model, the processes of nonlinear conversion of $RKE^{(>)}$ to $RKE^{(<)}$ and sweeping of the smaller scales by the larger ones are still included in the modeled dynamics. We will sketch the LES- α approach in this subsection and extract the subgrid models used in this study. For more details and applications of this approach, see [13]–[17], [23]–[26].

It is well known that the Navier-Stokes equations satisfy Kelvin’s circulation theorem, i.e.,

$$\frac{d}{dt} \oint_{\gamma(\mathbf{u})} u_j \, dx_j = \oint_{\gamma(\mathbf{u})} \frac{1}{Re} \partial_{kk} u_j \, dx_j \quad (28)$$

Here $\gamma(\mathbf{u})$ represents a fluid loop that moves with the Eulerian fluid velocity $\mathbf{u}(\mathbf{x}, t)$. The basic equations in the LES- α modeling may be introduced by modifying the velocity field by which the fluid loop is transported. The governing LES- α equations will provide the smoothed solution $\{v_j, P\}$ and we specify the equations for \mathbf{v} through the Kelvin-filtered circulation theorem. Namely, we integrate an approximately ‘defiltered’ velocity \mathbf{w} around a loop $\gamma(\mathbf{v})$ that moves with the regularized spatially filtered fluid velocity \mathbf{v} , cf. [23], [24], [27]

$$\frac{d}{dt} \oint_{\gamma(\mathbf{v})} w_j \, dx_j = \oint_{\gamma(\mathbf{v})} \frac{1}{Re} \partial_{kk} w_j \, dx_j \quad (29)$$

Hence, the basic transport properties of the LES- α model arise from filtering the ‘loop-velocity’ to obtain \mathbf{v} , then approximately defiltering \mathbf{v} to obtain the velocity \mathbf{w} in the Kelvin integrand. As we shall show, this approach will yield the model stress tensor m_{ij} needed to complete the filtering approach outlined in section 2.1. Direct calculation of the time derivative in this modified circulation theorem yields the Kelvin-filtered Navier-Stokes equations,

$$\partial_t w_i + v_j \partial_j w_i + w_k \partial_i v_k + \partial_i \hat{P} - \frac{1}{Re} \partial_{jj} w_i = 0, \quad \partial_j v_j = 0 \quad (30)$$

where we introduce the scalar function \hat{P} in removing the loop integral. The relation between the ‘defiltered’ velocity components w_i and the

LES- α velocity components v_i of the Kelvin loop needs to be specified separately. The Helmholtz defiltering operation was introduced in [10], [11] for this purpose:

$$w_i = v_i - \alpha^2 \partial_{jj} v_i = (1 - \alpha^2 \partial_{jj}) v_i = \mathcal{H}_\alpha(v_i) \quad (31)$$

where \mathcal{H}_α denotes the Helmholtz operator. We recall that all explicit filter operations L with a non-zero second moment, have a Taylor expansion whose leading order terms are of the same form as (31). Consequently, we infer that the leading order relation between α and Δ follows as $\alpha^2 = \Delta^2/24$ for the top-hat and the Gaussian filter. We will use this as the definition of α in the sequel.

The LES- α equations can be rearranged into a form similar to the basic LES equations (27), by splitting off a subgrid model for the turbulent stress tensor. For the Helmholtz defiltering, we obtain from (30):

$$\partial_t v_i + \partial_j(v_i v_j) + \partial_i P + \partial_j m_{ij}^\alpha - \frac{1}{Re} \partial_{jj} v_i = 0, \quad \partial_j v_j = 0 \quad (32)$$

after absorbing gradient terms into the redefined pressure P . Thus, we arrive at the following parameterization for the turbulent stress tensor

$$\mathcal{H}_\alpha(m_{ij}^\alpha) = \alpha^2 \left(\partial_k v_i \partial_k v_j + \partial_k v_i \partial_j v_k - \partial_i v_k \partial_j v_k \right) \quad (33)$$

In the evaluation of the LES- α dynamics in the above formulation, an inversion of the Helmholtz operator \mathcal{H}_α is required. The ‘exponential’ (or ‘Yukawa’) filter [52] is the exact, explicit filter which inverts \mathcal{H}_α . Thus, an inversion of \mathcal{H}_α corresponds to applying the exponential filter to the right-hand side of (33) in order to find m_{ij}^α . However, since the Taylor expansion of the exponential filter is identical at quadratic order to that of the top-hat and the Gaussian filters, we will approximate the inverse of \mathcal{H}_α by an application of the explicit top-hat filter, for reasons of computational efficiency. Moreover, in actual simulations the numerical realization of the exponential filter is only approximate and can just as well be replaced by the numerical top-hat filter. This issue of (approximately) inverting the Helmholtz operator will be studied separately and published elsewhere [37].

The full LES- α subgrid model m_{ij}^α has three distinct contributions. The first term on the right-hand side is readily recognized as the nonlinear gradient model which we will denote by A_{ij} . This term is closely related to the similarity model proposed by Bardina [28], as will be shown in the next subsection. The second term will be denoted by B_{ij} and combined with the first term, corresponds to the Leray regularization of the convective terms in the Navier-Stokes equations. This regularization

arises if the familiar contribution $u_j \partial_j u_i$ in the Navier-Stokes equations is replaced by $\bar{v}_j \partial_j v_i$ in the smoothed description. The third term will be denoted by C_{ij} . Further details of the derivation and mathematical properties of the LES- α model will be published elsewhere [37]. We can explicitly write the stress tensor for the LES- α model as

$$\begin{aligned} m_{ij}^\alpha &= \frac{\Delta^2}{24} \left(\overline{\partial_k v_i \partial_k v_j} + \overline{\partial_k v_i \partial_j v_k} - \overline{\partial_i v_k \partial_j v_k} \right) \\ &= \overline{A_{ij}} + \overline{B_{ij}} - \overline{C_{ij}} \end{aligned} \quad (34)$$

The explicit filter, represented by the overbar in this expression, is realized by the numerical top-hat filter in this study. It does not necessarily have to coincide with the LES-filter. While the LES-filter specifies the relation between the Navier-Stokes solution u_i and the LES- α solution v_i , the explicit LES- α filter is used to approximate \mathcal{H}_α^{-1} . We will consider the effects associated with variations in the filter-width $\tilde{\Delta}$ of the explicit LES- α filter with filter-width $\tilde{\Delta}/\Delta = \kappa$. Typical values that will be considered are $\kappa = 1$ and $\kappa = 2$.

In the next subsection we will describe some familiar subgrid models used in LES which are based on the similarity and eddy-viscosity concepts.

2.3. Similarity modeling and eddy-viscosity regularization

We distinguish two main contributions in present-day traditional subgrid modeling of the turbulent stress tensor, i.e., dissipative and similarity subgrid models. In this subsection we briefly describe these two basic approaches, as well as subgrid models that consist of combinations of an eddy-viscosity and a similarity part, so-called mixed models. The relative importance of the two components in such mixed models is obtained by using the dynamic procedure which is based upon Germano's identity (25). This mixed approach effectively regularizes and stabilizes similarity models.

As a result of the filtering, flow features of length-scales (much) smaller than the filter-width Δ are considerably attenuated. This implies that the natural molecular dissipation arising from the viscous fluxes, is strongly reduced, compared to the unfiltered flow-problem. In order to compensate for this, dissipative subgrid-models have been introduced to model the turbulent stress tensor. The prime example of such eddy-viscosity models is the Smagorinsky model [2, 53]:

$$m_{ij}^S = -(C_S \Delta)^2 |\sigma(\mathbf{v})| \sigma_{ij}(\mathbf{v}) \quad \text{with} \quad |\sigma(\mathbf{v})|^2 = \frac{1}{2} \sigma_{ij}(\mathbf{v}) \sigma_{ij}(\mathbf{v}) \quad (35)$$

where σ_{ij} is the strain rate, introduced above ($\sigma_{ij} = \partial_i v_j + \partial_j v_i$). This model adds only little computational overhead. The major short-coming of the Smagorinsky model is its excessive dissipation in laminar regions with mean shear, because σ_{ij} is large in such regions [36]. Furthermore, the correlation between the Smagorinsky model and the actual turbulent stress is quite low (reported to be ≈ 0.3 in several flows).

In trying to compensate for these short-comings of the Smagorinsky model, a second main branch of subgrid models emerges from the similarity concept [28]. Using the commutator notation, the turbulent stress tensor can be expressed as $\tau_{ij}(\mathbf{u}) = [L, S](u_i, u_j)$. In terms of this short-hand notation, the basic similarity model can be written as

$$m_{ij}^B = [L, S](v_i, v_j) \quad (36)$$

i.e., directly following the definition of the turbulent stress tensor, but expressed in terms of the available modeled LES velocity field. Generalizations of this similarity model arise by replacing v_i in (36) by an approximately defiltered field $\hat{v}_i = \mathcal{L}(v_i)$ where $\mathcal{L}(L(u)) \approx u$, i.e., \mathcal{L} approximates the ‘inverse’ of the filter L [49]. In detail, a generalized similarity model arises from $m^G = [L, S](\mathcal{L}^{-1}(v))$ using the approximate inversion. This approach is also known as the deconvolution model [54] and is reminiscent to the subgrid estimation model [55]. The correlation with τ_{ij} is much better with correlation coefficients reported in the range 0.6 to 0.9 in several flows. The low level of dissipation associated with these models renders them quite sensitive to the spatial resolution. At relatively coarse resolutions, the low level of dissipation can give rise to instability of the simulations. Moreover, these models add significantly to the required computational effort. At suitable resolution, however, the predictions arising from generalized similarity models are quite accurate.

An interesting subgrid model which follows the similarity approach to some degree and avoids the costly additional filter-operations is the nonlinear gradient model, mentioned earlier. This model can be derived from the Bardina scale-similarity model by using Taylor expansions of the filtered velocity. One may arrive at $\tau_{ij} = \frac{1}{12} \sum_k \Delta_k^2 (\partial_k \bar{u}_i) (\partial_k \bar{u}_j) + \mathcal{O}(\Delta^4)$. The first term on the right-hand side is referred to as the ‘nonlinear gradient model’ or tensor-diffusivity model:

$$m_{ij}^{TD} = \frac{1}{24} \sum_k \Delta_k^2 (\partial_k v_i) (\partial_k v_j) \quad (37)$$

Since this model is part of all three different LES- α models identified in the previous subsection, we will analyze the dynamics and the instabilities arising from this model in some more detail in the next subsection.

The three subgrid models, i.e., (35), (36) and (37) constitute well-known examples in LES-literature, which represent basic dissipative and reactive, or dispersive, properties of subgrid models for the turbulent stress tensor. These basic similarity and eddy-viscosity models can be combined in mixed models using the dynamic procedure, which provides a way of combining the two basic components of a mixed model without introducing additional external ad hoc parameters.

We consider simple mixed models based on eddy-viscosity and similarity. In these models the eddy-viscosity component reflects local turbulence activities and the local value of the eddy-viscosity adapts itself to the instantaneous flow. The dynamic procedure starts from Germano's identity (25). A common way to write Germano's identity is:

$$T_{ij} - \widehat{\tau_{ij}} = R_{ij} \quad (38)$$

where

$$T_{ij} = \widehat{u_i u_j} - \widehat{\bar{u}_i} \widehat{\bar{u}_j} \quad (39)$$

$$R_{ij} = (\widehat{\bar{u}_i \bar{u}_j}) - \widehat{\bar{u}_i} \widehat{\bar{u}_j} \quad (40)$$

Here, in addition to the basic LES-filter $\overline{(\cdot)}$ of width $\overline{\Delta}$ a so-called 'test'-filter $\widehat{(\cdot)}$ of width $\widehat{\Delta}$ is introduced. Usually, this test-filter is wider than the LES-filter and the combined filter $\widehat{(\cdot)}$ has a width that follows from $\widehat{\Delta}^2 = \widehat{\Delta}^2 + \overline{\Delta}^2$. This relation is exact for the composition of two Gaussian filters and can be shown to be 'optimal' for other filters such as the top-hat filter [7]. The only external parameter that needs to be specified in the dynamic procedure is the ratio $\widehat{\Delta}/\overline{\Delta}$ which is commonly set equal to two. The terms at the left-hand side of the Germano identity (38) are the turbulent stress tensor on the 'combined' filter level (T_{ij}) and the turbulent stress tensor, filtered with the test-filter ($\widehat{\tau_{ij}}$), respectively. Finally, R_{ij} represents the resolved stress tensor which can be explicitly calculated using the modeled LES fields.

The general procedure for obtaining 'locally' optimal model parameters in a mixed formulation starts by assuming a basic model m_{ij} to approximate the turbulent stress tensor τ_{ij} , and a corresponding model M_{ij} for T_{ij} . We consider m_{ij} to be of 'mixed' type, i.e.,

$$m_{ij} = a_{ij} + c b_{ij} \quad (41)$$

where a_{ij} and b_{ij} are basic models. These basic models involve operations on \mathbf{v} only; $a_{ij} = a_{ij}(\mathbf{v})$, $b_{ij} = b_{ij}(\mathbf{v})$. Furthermore, in standard mixed models, c is a scalar coefficient-field which is to be determined.

The model M_{ij} is represented as:

$$M_{ij} = A_{ij} + CB_{ij} \quad (42)$$

where $A_{ij} = a_{ij}(\hat{\mathbf{v}})$, $B_{ij} = b_{ij}(\hat{\mathbf{v}})$. It is essential in this formulation that the coefficient C corresponding to the composed filter-level is well approximated by the coefficient c ; i.e., we assume $C \approx c$. Insertion in Germano's identity yields $M_{ij} + \widehat{m_{ij}} = R_{ij}$, or in more detail,

$$(A_{ij} + \widehat{a_{ij}}) + c[B_{ij} + \widehat{b_{ij}}] = R_{ij} \quad (43)$$

where we have used the approximation $\widehat{cb_{ij}} \approx \widehat{c}\widehat{b_{ij}}$. Introducing the short-hand notation $\mathcal{A}_{ij} = A_{ij} + \widehat{a_{ij}}$, $\mathcal{B}_{ij} = B_{ij} + \widehat{b_{ij}}$, the coefficient c is required to obey $c\mathcal{B}_{ij} = R_{ij} - \mathcal{A}_{ij}$. This relation should hold for all tensor-components, which of course is not possible for a scalar coefficient field c . To resolve this situation we introduce an averaging operator $\langle f \rangle$ and define the 'Germano-residual' by

$$\varepsilon(c) = \langle \frac{1}{2} \{ (R_{ij} - \mathcal{A}_{ij}) - c\mathcal{B}_{ij} \}^2 \rangle \quad (44)$$

From this we obtain an optimality condition for c from $\varepsilon'(c) = 0$ and we can solve the local coefficient as

$$c = \frac{\langle (R_{ij} - \mathcal{A}_{ij})\mathcal{B}_{ij} \rangle}{\langle \mathcal{B}_{ij}\mathcal{B}_{ij} \rangle} \quad (45)$$

where we assumed $\langle c f g \rangle \approx c \langle f g \rangle$. The averaging operator $\langle f \rangle$ is usually defined in terms of an integration over homogeneous directions of the flow-domain. In the case of the mixing layer, considered here, the averaging over the homogeneous streamwise and spanwise direction results in a dynamic coefficient c which is a function of the normal coordinate x_2 and time t . In more complex flow-domains, averaging over homogeneous directions may no longer be possible. Taking a running-average over time t is then a viable alternative, as was recently established, e.g., for flow in a spatially developing mixing layer [35].

As an example we consider the Smagorinsky model as the base model. The corresponding models on the two filter-levels can be written as

$$m_{ij}^D = -C_d \overline{\Delta}^2 |\sigma(\mathbf{v})| \sigma_{ij}(\mathbf{v}) ; \quad M_{ij}^D = -C_d \widehat{\overline{\Delta}}^2 |\sigma(\hat{\mathbf{v}})| \sigma_{ij}(\hat{\mathbf{v}}) \quad (46)$$

The 'optimal' C_d follows from $C_d = \langle R_{ij}\mathcal{B}_{ij} \rangle / \langle \mathcal{B}_{ij}\mathcal{B}_{ij} \rangle$. In order to prevent numerical instability caused by negative values of C_d , the model coefficient C_d is artificially set to zero at locations where the procedure would return negative values. Sometimes, in developing flows, it

is beneficial to also introduce a ‘ceiling’-value for C_d . This value should be chosen such that once the flow is well-developed in time the actual limitation arising from the ceiling-value is no longer restrictive [35].

The dynamic mixed model employs the sum of Bardina’s similarity and Smagorinsky eddy-viscosity model as the base model, i.e.,

$$m_{ij}^{DM} = [L, S](v_i, v_j) - C_d \bar{\Delta}^2 |S(\mathbf{v})| S_{ij}(\mathbf{v}) \quad (47)$$

Likewise, a mixed nonlinear gradient model can be introduced by

$$m_{ij}^{DG} = \frac{1}{24} \bar{\Delta}^2 (\partial_k v_i)(\partial_k v_j) - C_d \bar{\Delta}^2 |S(\mathbf{v})| S_{ij}(\mathbf{v}) \quad (48)$$

The dynamic procedure has been used in a number of different flows. Compared to predictions using only the constitutive base models, the dynamic procedure generally enhances the accuracy and robustness. Moreover, it responds to the developing flow in such a way that the eddy-viscosity is strongly reduced in laminar regions and near solid walls [56]. This avoids specific modeling of transitional regions and near-wall phenomena, provided the resolution is sufficient. At even coarser resolution one may have to resort to specific models for transition and walls. We will not enter into this problem. Rather, we will focus on the properties of the nonlinear gradient model in the next subsection.

2.4. Analysis of instabilities of the nonlinear gradient model in one dimension

From the discussion of the previous two subsections, it would appear that the nonlinear gradient subgrid model would be very well suited to parameterize the dynamic effects of the small scales in a turbulent flow. This model is part of the full LES- α model and it also emerges as a Taylor expansion of the Bardina similarity model. In this subsection we will analyse the nonlinear gradient model in the context of the one-dimensional Burgers equation and show that this model gives rise to very strong instabilities. Apparently, some features appear to be missing in the pure nonlinear gradient model. In subsequent sections we will show in what way the explicit filtering and the other terms in the LES- α model, or dynamic eddy-viscosity regularization, alter this peculiar behavior of the nonlinear gradient model.

We will analyse the nature of the instability of the pure gradient model for the one-dimensional Burgers equation [31]. The linear stability of a sinusoidal profile will be investigated. If a flow is linearly unstable then it is nonlinearly unstable to arbitrarily small initial disturbances. The linear analysis thus provides some information on the nonlinear equation.

The Burgers equation with gradient subgrid-model is written as:

$$\partial_t u + \frac{1}{2} \partial_x (u^2) - \nu \partial_x^2 u = -\frac{1}{2} \eta \partial_x (\partial_x u)^2 + f(x) \quad (49)$$

The parameter $\eta = \Delta^2/12$. The following analysis shows that smooth solutions of equation (49) can be extremely sensitive to small perturbations, leading to severe instabilities. In particular, we consider the linear stability of a 2π -periodic, stationary solution, $U(x, t) = \sin(x)$ on the domain $[0, 2\pi]$ with periodic boundary conditions. The forcing function f is determined by the requirement that U is a solution of equation (49). We substitute a superposition of U and a perturbation w ,

$$u(x, t) = U(x) + w(x, t) \quad (50)$$

into equation (49) and linearize around U , omitting higher order terms in w :

$$\partial_t w + (1 - \eta) \sin(x) \partial_x w + (w + \eta \partial_x^2 w) \cos(x) = \nu \partial_x^2 w \quad (51)$$

We use a Fourier expansion for w written as $w = \sum \alpha_k(t) e^{ikx}$. After substitution of this series into equation (51) we obtain an infinite system of ordinary differential equations for the Fourier coefficients α_k :

$$\dot{\alpha}_k = \frac{1}{2}k(\eta k - \eta - 1)\alpha_{k-1} - k^2\nu\alpha_k + \frac{1}{2}k(\eta k + \eta + 1)\alpha_{k+1} \quad (52)$$

To understand the nature of the nonlinear gradient model for the Burgers equation, we first analyse system (52) assuming $\nu = 0$. Instead of the infinite system, we consider a sequence of finite dimensional systems,

$$\dot{\mathbf{z}}_n = M_n \mathbf{z}_n \quad (53)$$

where \mathbf{z}_n is a vector containing the $2n + 1$ Fourier coefficients $\alpha_{-n} \dots \alpha_n$ and M_n is a $(2n + 1) \times (2n + 1)$ tri-diagonal matrix:

with

$$l_k = \frac{1}{2}k(\eta k - \eta - 1) \quad ; \quad r_k = \frac{1}{2}(k - 1)(\eta k + 1) \quad (55)$$

The eigenvalues of M_n determine the stability of the problem. The system is unstable if the maximum of the real parts of the eigenvalues is positive. We denote the eigenvalues of M_n by λ_j and introduce λ_{max} such that

$$|\lambda_{max}| = \max_j |\lambda_j| \quad (56)$$

This eigenvalue problem can be shown to have the following asymptotic properties (for a detailed proof see [31]):

1. if λ is an eigenvalue then $-\lambda$ is an eigenvalue

2. $|\lambda_{max}| \sim \eta n^2$

3. $|\text{Im}(\lambda_{max})| \leq n - 1$

The first point implies that λ_{max} can be chosen such that $\text{Re}(\lambda_{max}) \geq 0$. Hence, the combination of these three properties yields the asymptotic behavior of the maximum of the real parts of the eigenvalues:

$$\text{Re}(\lambda_{max}) \sim \eta n^2 \quad (60)$$

This shows that the inviscid system is linearly unstable and that the largest real part of the eigenvalues is asymptotically proportional to n^2 , where n is the number of Fourier modes taken into account.

It should be observed that the instability is severe, since the system is not only unstable, but the growth rate of the instability is infinitely large as $n \rightarrow \infty$. The instability is fully due to the incorporation of the gradient model, since all eigenvalues of the matrix M_n are purely imaginary in case the inviscid Burgers equation without subgrid-model is considered ($\eta = 0$). In numerical simulations the instability will grow with a finite speed, since then the number of Fourier modes is limited by the finite grid. Moreover, expression (60) illustrates that grid-refinement (with η kept constant), which corresponds to a larger n , will not stabilize the system, but rather enhance the instability. The growth rate of the instability of the one-dimensional problem can be expressed in terms of Δ and the grid-spacing h : $\eta n^2 \sim (\Delta/h)^2$. Consequently, the instability is not enhanced if the ratio between Δ and h is kept constant.

Finally, we will consider the more complicated case $\nu \neq 0$. The linear system in equation (52) now gives rise to matrices M_n which have a negative principal diagonal. It is known that for every fixed value of n there exists an eigenvalue arbitrarily close to the eigenvalue of the

inviscid system (λ_{max}) if ν is sufficiently small [57]. Hence for small values of ν the viscous system for finite n is still linearly unstable. The matrix M_n is strictly diagonally dominant if $\nu > \eta + 1$, while all rows except n and $n+2$ are already diagonally dominant if $\nu > \eta$. If the matrix is diagonally dominant, the real parts of all eigenvalues are negative and, consequently, the system is stable. This indicates that stability can be achieved by a sufficiently large viscosity, which does not depend on n , but only on η . Thus, if the gradient model is supplemented with an adequate eddy-viscosity the instability will be removed as is the case with a dynamic mixed model involving the gradient model.

3. Numerical simulations of a turbulent mixing layer

In this section we first present the numerical methods used to solve the DNS and LES equations (subsection 3.1). We illustrate the accuracy of these methods for turbulent flow in a mixing layer in subsection 3.2.

3.1. Time-integration and spatial discretization

The Navier-Stokes or modeled LES equations are discretized using the so-called method of lines. We consider the compressible formulation and perform simulations at a low convective Mach number which was shown to provide essentially incompressible flow-dynamics. The method of lines allows to treat the spatial and temporal discretization separately and gives rise to a large number of ordinary differential equations for the unknowns on a computational grid.

We write the Navier-Stokes or LES equations concisely as $\partial_t \mathcal{U} = \mathcal{F}(\mathcal{U})$ where \mathcal{U} denotes the state-vector containing, e.g., velocity and pressure, and \mathcal{F} is the total flux, composed of the convective, the viscous, and possibly the subgrid fluxes. The operator \mathcal{F} contains first and second order partial derivatives with respect to the spatial coordinates x_j . The equations are discretized on a uniform rectangular grid and the grid size in the x_j -direction is denoted by h_j . If we adopt a specific spatial discretization around a grid point \mathbf{x}_{ijk} , the operator $\mathcal{F}(\mathcal{U})$ is approximated in a consistent manner by an algebraic expression $F_{ijk}(\{U_{\alpha\beta\gamma}\})$ where $\{U_{\alpha\beta\gamma}\}$ denotes the state vectors in all the grid-points, labeled by α, β, γ . Usually, only neighboring grid points around (i, j, k) appear explicitly in F_{ijk} , e.g., in case finite difference or finite volume discretizations are considered. After applying the method of lines, the governing equations yield

$$d_t U_{ijk}(t) = F_{ijk}(\{U_{\alpha\beta\gamma}\}) \quad ; \quad U_{ijk}(0) = U_{ijk}^{(0)} \quad (61)$$

where $U_{ijk}^{(0)}$ represents the initial condition. Hence, in order to specify the numerical treatment, apart from the initial and boundary conditions, the spatial discretization which gives rise to F_{ijk} and the temporal integration need to be specified. We next introduce these separately.

The time stepping method which we adopt is an explicit four-stage compact-storage Runge-Kutta method. When we consider the scalar differential equation $du/dt = f(u)$, this Runge-Kutta method performs within one time step of size δt

$$u^{(j)} = u^{(0)} + \beta_j \delta t f(u^{(j-1)}) \quad (j = 1, 2, 3, 4) \quad (62)$$

with $u^{(0)} = u(t)$ and $u(t + \delta t) = u^{(4)}$. With the coefficients $\beta_1 = 1/4$, $\beta_2 = 1/3$, $\beta_3 = 1/2$ and $\beta_4 = 1$ this yields a second-order accurate time integration method [58]. The time step is determined by the stability restriction of the numerical scheme. It depends on the grid-size h and the eigenvalues of the flux Jacobi matrix of the numerical flux f . In a short-hand notation one may write $\delta t = \text{CFL } h/|\lambda_{\max}|$ where $|\lambda_{\max}|$ denotes the eigenvalue of the flux Jacobi matrix with maximal size, and CFL denotes the Courant-Friedrichs-Levy-number which depends on the specific choice of explicit time integration method. For the present four-stage Runge-Kutta method a maximum CFL number of 2.4 can be established using a Von Neumann stability analysis. In the actual simulations we use $\text{CFL} = 1.5$, which is suitable for both DNS and LES, irrespective of the specific subgrid model used.

In order to specify the spatial discretization we distinguish between the treatment of the convective and the viscous fluxes. We will only specify the numerical approximation of the ∂_1 -operator; the ∂_2 and ∂_3 -operators are treated analogously. Subgrid-terms are discretized with the same method as the viscous terms. Throughout we will use a second order method for the viscous fluxes and both a second order, and a fourth order accurate method for the convective fluxes. All these methods are constructed from (a combination of) first order numerical derivative operators D_j .

The second-order method that we consider is a finite volume method [59]. The discretization of the convective terms is the cell vertex trapezoidal rule, which is a weighted second-order central difference. In vertex (i, j, k) the corresponding operator is denoted by D_1 and for the approximation of $\partial_1 f$ it is defined as

$$\begin{aligned} (D_1 f)_{i,j,k} &= (s_{i+1,j,k} - s_{i-1,j,k})/(2h_1) \\ \text{with } s_{i,j,k} &= (g_{i,j-1,k} + 2g_{i,j,k} + g_{i,j+1,k})/4 \\ \text{and } g_{i,j,k} &= (f_{i,j,k-1} + 2f_{i,j,k} + f_{i,j,k+1})/4 \end{aligned} \quad (63)$$

The viscous terms contain second-order derivatives which are treated by a consecutive application of two first order numerical derivatives. This requires for example that the gradient of the velocity is calculated in centers of grid-cells. In center $(i + \frac{1}{2}, j + \frac{1}{2}, k + \frac{1}{2})$ the corresponding discretization $D_2 f$ has the form

$$(D_2 f)_{i+\frac{1}{2}, j+\frac{1}{2}, k+\frac{1}{2}} = (s_{i+1, j+\frac{1}{2}, k+\frac{1}{2}} - s_{i, j+\frac{1}{2}, k+\frac{1}{2}})/h_1 \quad (64)$$

with $s_{i, j+\frac{1}{2}, k+\frac{1}{2}} = (f_{i, j, k} + f_{i, j+1, k} + f_{i, j, k+1} + f_{i, j+1, k+1})/4$

The second derivative is subsequently calculated with operator D_1 ; thus we approximate, e.g., $\partial_{11}(f)_{ijk} \approx D_1(D_2(f))_{ijk}$.

The combination of D_1 and D_2 is robust with respect to odd-even decoupling but it is only second order accurate. In a similar manner we may construct a fourth-order accurate method. The corresponding expression for $D_3 f$ has the following form:

$$(D_3 f)_{i, j, k} = (-s_{i+2, j, k} + 8s_{i+1, j, k} - 8s_{i-1, j, k} + s_{i-2, j, k})/(12h_1) \quad (65)$$

with $s_{i, j, k} = (-g_{i, j-2, k} + 4g_{i, j-1, k} + 10g_{i, j, k} + 4g_{i, j+1, k} - g_{i, j+2, k})/16$
and $g_{i, j, k} = (-f_{i, j, k-2} + 4f_{i, j, k-1} + 10f_{i, j, k} + 4f_{i, j, k+1} - f_{i, j, k+2})/16$

This scheme is conservative, since it is a weighted central difference. The coefficients in the definition for $g_{i, j, k}$ are chosen such that $g_{i, j, k}$ is a fourth order accurate approximation to $f_{i, j, k}$ and π -waves in the x_3 -direction give no contributions to $g_{i, j, k}$. The definition for $s_{i, j, k}$ has the same properties with respect to the x_2 -direction. For convenience, we will refer to a combination of D_3 for the convective, and D_1 , D_2 for the viscous fluxes as fourth-order methods, but we remark that the formal spatial accuracy of the scheme is only second-order due to the treatment of the viscous terms.

3.2. The turbulent mixing layer

The flow in a temporally developing turbulent mixing layer is well documented in literature (e.g. [7]), and will be considered here to test the LES- α modeling approach. In this section we review the scenario of the development of the flow that is considered and sketch the type of predictions that can be obtained by traditional LES using the dynamic model. This serves as a point of reference for the next section.

We simulate the compressible three-dimensional temporal mixing layer and use a convective Mach number $M = 0.2$ and a Reynolds number based on upper stream velocity and half the initial vorticity thickness of 50. The governing equations are solved in a cubic geometry of side $l = 59$. Periodic boundary conditions are imposed in the streamwise

(x_1) and spanwise (x_3) direction, while in the normal (x_2) direction the boundaries are free-slip walls. The initial condition is formed by mean profiles corresponding to constant pressure $p = 1/(\gamma M^2)$ where $\gamma = 1.4$ is the adiabatic gas constant, $u_1 = \tanh(x_2)$ for the streamwise velocity component, $u_2 = u_3 = 0$ and a temperature profile given by the Busemann-Crocco law. Superimposed on the mean profile are two- and three-dimensional perturbation modes obtained from linear stability theory. Further details may be found in [34].

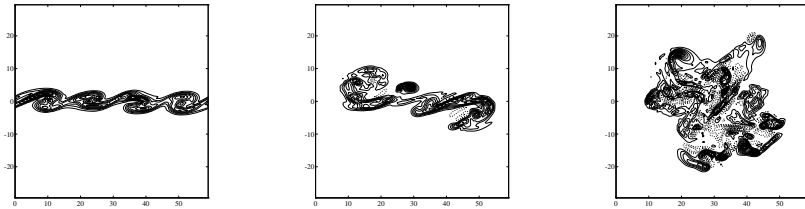


Figure 1. Results from a DNS using 192^3 points. Contours of spanwise vorticity for the plane $x_3 = 3L/4$ at $t = 20$, $t = 40$ and $t = 80$ from left to right. Solid and dotted contours indicate negative and positive vorticity respectively. The contour increment is 0.1.

The DNS is conducted on a uniform grid with 192^3 cells using the fourth order spatial discretization method. Visualization of the DNS data demonstrates the roll-up of the fundamental instability and successive pairings (figure 1). Four rollers with mainly negative spanwise vorticity are observed at $t = 20$. After the first pairing ($t = 40$) the flow has become highly three-dimensional. Another pairing ($t = 80$), yields a single roller in which the flow exhibits a complex structure.

The accuracy of the simulation with 192^3 cells is satisfactory as is inferred from coarser grid computations on 64^3 and 128^3 cells. The evolution of the momentum thickness

$$\delta(t) = \frac{1}{4} \int_{-L/2}^{L/2} (1 - \langle u_1 \rangle)(\langle u_1 \rangle + 1) dx_2 \quad (66)$$

and an instantaneous velocity component at the center of the shear layer are shown in figure 2. The 64^3 -simulation is inadequate for the prediction of the local instantaneous solution, but the momentum thickness appears quite reasonable.

To illustrate the effect that filtering has on a well-developed DNS solution, vorticity contours for $\Delta = L/16$ are shown in figure 3. Comparing this with the corresponding DNS results in figure 1 allows one to appreciate the strong smoothing effect that filtering has on the solution.

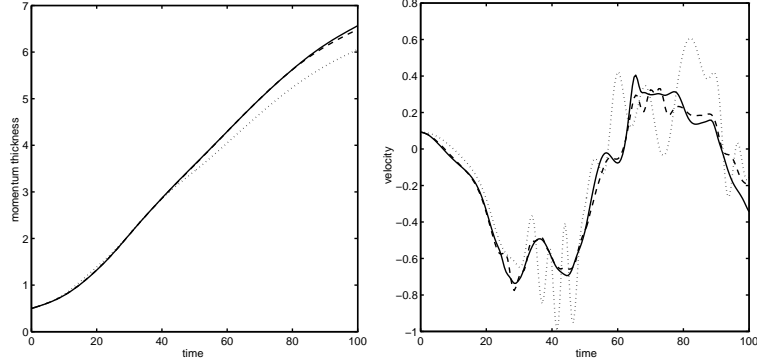


Figure 2. Evolution of the momentum thickness (left) and u_3 at $(\frac{1}{4}L, 0, \frac{1}{2}L)$ (right) obtained from simulations which do not involve any subgrid model and employ a sequence of grids: 64^3 (dotted), 128^3 (dashed) and 192^3 (solid).

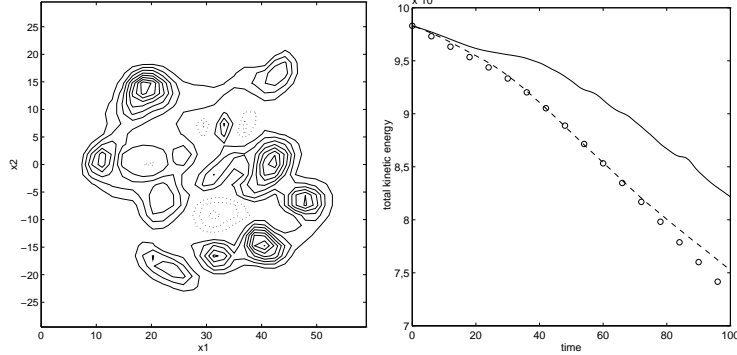


Figure 3. Left: Contour-lines of the z -component of the vorticity. The effect of spatially filtering the DNS solution at $t = 80$ in figure 1 with a top-hat filter and filter-width $\Delta = L/16$. Right: prediction of the kinetic energy with the dynamic eddy-viscosity model (dashed) compared with the filtered DNS results (markers) and a simulation on the coarse LES grid (32^3) without a model (solid).

On the right in figure 3 we included the decay of the resolved turbulent kinetic energy, defined as

$$E = \frac{1}{2} \int_{\Omega} (\bar{u}_1^2 + \bar{u}_2^2 + \bar{u}_3^2) \, d\mathbf{x} \quad (67)$$

We observe that the dynamic eddy-viscosity model generates quite a correction of the ‘no-model coarse grid simulation’. Other models were also considered in [7], such as Smagorinsky’s model, Bardina’s scale-similarity model and dynamic mixed models. Roughly speaking, the use of Bardina’s model leads to flow predictions which contain somewhat

too many small scale features whereas the Smagorinsky model, with eddy-coefficient $C_S = 0.17$ prevents the flow from developing beyond the transitional stage due to excessive dissipation in the early stages of the evolution. Finally, the dynamic mixed models were all shown to perform about equally well and provide accurate predictions.

4. LES- α of a mixing layer

In this section we will consider LES using the LES- α model. Above, in section 2.2, we introduced this model and identified three distinct contributions; in fact, the LES- α model contains the explicitly filtered nonlinear gradient model (m_{ij}^{NG}), the Leray model (m_{ij}^L) and the complete LES- α model (m_{ij}^α). These are defined as

$$m_{ij}^{NG} = \frac{\Delta^2}{24} \left(\overline{\partial_k v_i \partial_k v_j} \right) \equiv \overline{A_{ij}} \quad (68)$$

$$m_{ij}^L = \frac{\Delta^2}{24} \left(\overline{\partial_k v_i \partial_k v_j} + \overline{\partial_k v_i \partial_j v_k} \right) \equiv \overline{A_{ij}} + \overline{B_{ij}} \quad (69)$$

$$\begin{aligned} m_{ij}^\alpha &= \frac{\Delta^2}{24} \left(\overline{\partial_k v_i \partial_k v_j} + \overline{\partial_k v_i \partial_j v_k} - \overline{\partial_i v_k \partial_j v_k} \right) \\ &\equiv \overline{A_{ij}} + \overline{B_{ij}} - \overline{C_{ij}} \end{aligned} \quad (70)$$

First we will consider reference LES using these models and compare predictions with those obtained with dynamic subgrid models (subsection 4.1). Then we focus our attention on the resolved kinetic energy dynamics in subsection 4.2. Finally, in subsection 4.3 we consider (nearly) grid-independent LES- α predictions which arise when refining the grid while keeping Δ constant.

4.1. Reference LES of the mixing layer

In order to create a point of reference, we consider LES defined on a resolution of 32^3 grid-points. This choice represents a significant saving compared to the full DNS and places a considerable importance on the subgrid fluxes. This resolution was used previously in a comparative study of subgrid models in [7].

The simulations will be illustrated by considering the evolution of the resolved kinetic energy $E(t)$, defined in (67). In addition, we consider the momentum thickness $\delta(t)$, based on filtered variables which quantifies the spreading of the mean velocity profile. We also investigate the Reynolds-stress profiles $\langle w_1 w_2 \rangle$ defined with respect to the fluctuation $w_i = v_i - \langle v_i \rangle$. Finally, we incorporate the streamwise kinetic energy spectrum in the turbulent regime at $t = 80$. In this way a number of essentially different quantities (mean, local, plane averaged) are included

in the comparisons in order to assess various aspects of the quality of the models.

For all simulations we will use a LES-filter-width $\Delta = L/16$. On the 32^3 grid this implies that $\Delta/h = 2$, i.e., two grid-intervals cover the filter-width. Moreover, unless explicitly stated otherwise, the explicit filter used in the definition of the LES- α subgrid models will have the same width as the LES-filter, i.e., $\kappa = 1$. The filtering is done using the top-hat filter and we adopt the trapezoidal rule to perform the numerical integrations. The simulations that will be presented in the following subsections correspond to a slightly different initial condition than used in section 3.2. The differences are fairly small, but still prevent a direct comparison with the filtered DNS results presented in section 3.2.

Explicit filtering is essential. The proposed subgrid models in the α framework each contain the nonlinear gradient model and also involve an explicit filtering. As analyzed in section 2.4, the nonlinear gradient model, without explicit filtering gives rise to instabilities. These instabilities manifest themselves, e.g., by an increase in the resolved kinetic energy, instead of the monotonous decrease that is characteristic of this relaxing shear layer, cf. figure 3.

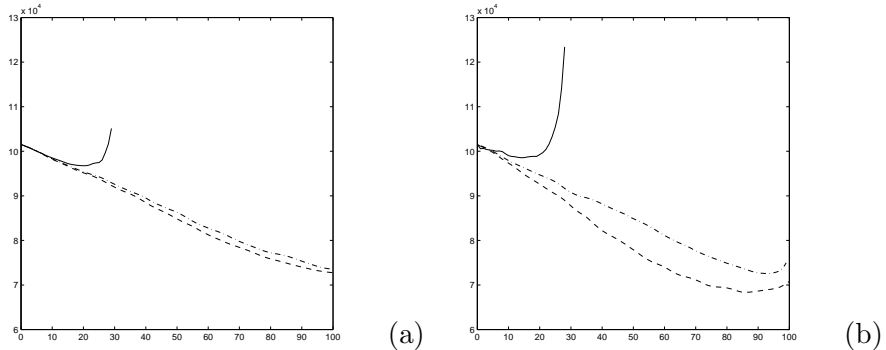


Figure 4. Evolution of resolved kinetic energy for the nonlinear gradient model (solid) and the filtered nonlinear gradient model, using $\kappa = 1$ (dashed) and $\kappa = 2$ (dash-dotted) (a). In (b) we show the corresponding results obtained with the unfiltered (solid) and filtered full LES- α model. These instabilities are expected on grounds discussed in subsection 2.4.

The question arises whether the explicit filtering can stabilize the simulations on this reference grid. In figure 4 we compiled predictions for the kinetic energy, obtained with the nonlinear gradient and the full LES- α model, both without and with explicit filtering, at different val-

ues of the ratio κ . We notice that the explicit filtering is essential in order to maintain stability of the simulation. It appears that the unfiltered LES- α model is even slightly more unstable than the unfiltered nonlinear gradient model. We also considered these models at a higher resolution of 64^3 grid-points. Consistent with the analysis in section 2.4 the instability becomes stronger if the grid is refined while keeping the LES filter-width Δ constant. It is seen that the value of κ , which defines the width of the explicit filter relative to the width of the LES filter, has a comparably small effect on the predictions of the nonlinear gradient model. The instabilities which arise when using the full LES- α model, appear somewhat stronger and, e.g., E even increases in the turbulent regime, despite the explicit filtering. This indicates a marginally unstable simulation, and the situation improves when κ is increased.

Reference LES- α predictions. Some basic predictions obtained using the three LES- α models will be presented next. These predictions will contain errors because of shortcomings in the subgrid parameterizations and the numerical treatment. These aspects will be focused upon in the next two subsections respectively; here it is our aim to provide an impression of the predictions under numerical conditions that are fairly common in present-day LES, e.g. $\Delta/h = 2$.

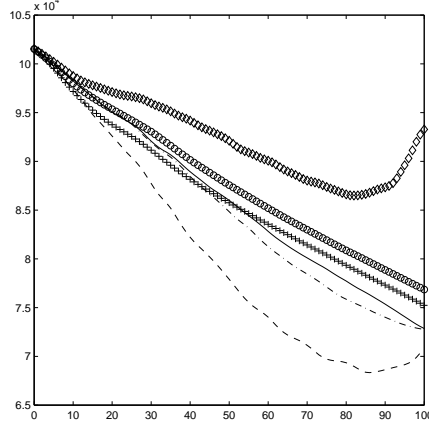


Figure 5. Evolution of the resolved kinetic energy E comparing the following models: LES- α (dashed), Leray (solid), filtered nonlinear gradient model (dash-dotted), dynamic mixed (+), dynamic eddy-viscosity (o) and no-model (\diamond). We used $\kappa = 1$.

In figure 5 we compare the evolution of the resolved turbulent kinetic energy E for a number of subgrid models. We included not only predictions corresponding to the three LES- α models, but also the dynamic mixed model, the dynamic eddy-viscosity model and the simula-

tion without any subgrid model at all. The subgrid models provide a significant improvement compared to the case without a model. From previous simulations we know that a fairly close agreement exists between filtered DNS data and the dynamic models, as shown in figure 3 (see [7] for more details). Using the dynamic predictions as point of reference here as well, we notice that the Leray and the filtered nonlinear gradient model provide more accurate predictions than the full LES- α model. We also considered the Bardina model and observed that the predictions are virtually identical to those obtained with the filtered nonlinear gradient model. The Smagorinsky model at $C_S = 0.17$ was used as well and showed too strong dissipation.

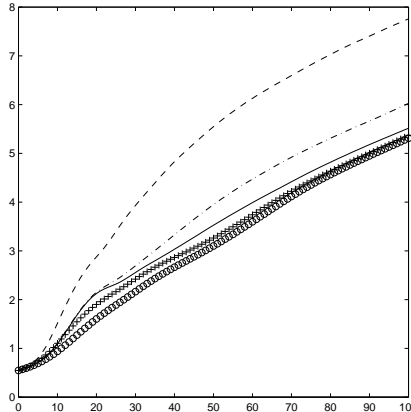


Figure 6. Evolution of the resolved momentum thickness δ comparing the following models: LES- α (dashed), Leray (solid), filtered nonlinear gradient model (dash-dotted), dynamic mixed (+), dynamic eddy-viscosity (o). We used $\kappa = 1$.

The momentum thickness δ is shown in figure 6. The prediction of δ from the full LES- α model is much higher than those obtained with the other subgrid models and compared to the dynamic model predictions as point of reference, it appears too high. The predictions of the Bardina similarity model again coincide with the filtered nonlinear gradient model, and these predictions are somewhat larger than those from the Leray model. All the LES- α models predict δ larger than the dynamic models. Since the dynamic predictions slightly underestimate δ according to [7], it appears that the Leray model and the filtered nonlinear gradient model predict δ more accurately, compared to filtered DNS results, than the other models.

In figure 7 we collected the Reynolds stress $-\langle w_1 w_2 \rangle$. We observe that all three LES- α models predict a considerably higher level of fluctuations compared to the dynamic models. The full LES- α model predicts levels

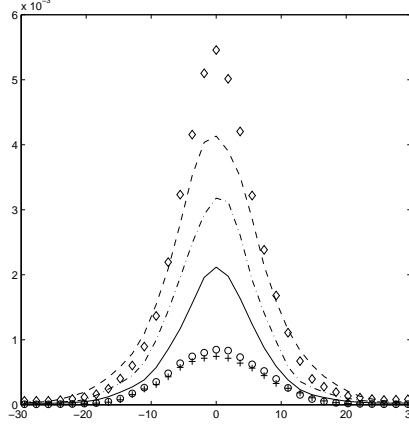


Figure 7. Comparison of the Reynolds stress $-\langle w_1 w_2 \rangle$ at $t = 70$: LES- α (dashed), Leray (solid), filtered nonlinear gradient model (dash-dotted), dynamic mixed (+), dynamic eddy-viscosity (o) and no-model (\diamond). We used $\kappa = 1$.

of fluctuation close to those obtained from the simulation without any subgrid model, suggesting that this model introduces too many small scales into the solution. Likewise, the filtered gradient model generates high levels of fluctuations, while the Leray model is much closer to the levels of fluctuation that are found using the dynamic models.

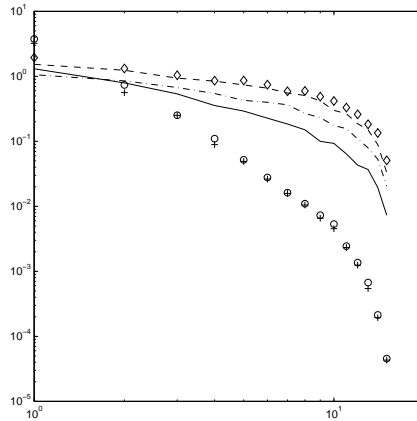


Figure 8. Comparison of the streamwise energy spectrum $A(k)$ at $t = 80$: LES- α (dashed), Leray (solid), filtered nonlinear gradient model (dash-dotted), dynamic mixed (+), dynamic eddy-viscosity (o) and no-model (\diamond). We used $\kappa = 1$.

We consider the streamwise kinetic energy spectrum in the turbulent regime at $t = 80$, in figure 8. We observe a clear separation of the predic-

tions in two groups. The two dynamic models show a strong reduction of the smaller scales. In contrast, the full LES- α model displays a spectrum that is quite close to the spectrum of the simulation without any subgrid model. This situation improves significantly for the filtered nonlinear gradient model and finally, the Leray model provides the largest attenuation of the small scales among the three LES- α models.

In summary, the simulations suggest that the full LES- α model does not sufficiently reduce the resolved kinetic energy, leads to too large momentum-thickness and too high levels of fluctuation, which is apparent in the spectrum at small scales and snapshots of the solution. The filtered nonlinear gradient model performs better than the full LES- α model but also over-predicts the smaller scales. In contrast to these two models, the Leray model, appears to predict the energy decay properly, shows accurate momentum-thicknesses and apparently reliable levels of turbulence intensities, as shown also in the spectrum and in snapshots of the solution. In order to better understand these predictions we turn to the resolved kinetic energy dynamics in the next subsection and consider the contribution of the individual terms in the models.

4.2. Resolved kinetic energy dynamics

In this section we consider the evolution of the resolved kinetic energy and determine the type and magnitude of the various subgrid contributions. The evolution of E is governed by

$$\begin{aligned}\partial_t E &= \int_{\Omega} \left\{ \frac{1}{Re} \bar{u}_i \partial_j \bar{\sigma}_{ij} - \bar{u}_i \partial_j \tau_{ij} \right\} d\mathbf{x} \\ &= \int_{\Omega} \left\{ -\frac{1}{2Re} \bar{\sigma}_{ij} \bar{\sigma}_{ij} + \tau_{ij} \partial_j \bar{u}_i \right\} d\mathbf{x}\end{aligned}\quad (71)$$

where use was made of the identity $\bar{\sigma}_{ij} \partial_j \bar{u}_i = \frac{1}{2} \bar{\sigma}_{ij} \bar{\sigma}_{ij}$. The predicted kinetic energy evolution, corresponding to a given LES model, emerges by replacing the turbulent stress tensor by its subgrid scale model. We notice that the dynamics of E is governed by a purely dissipative term arising from the molecular dissipation and a term that is associated with the subgrid model. We will consider the resolved energy dynamics both for the coarse reference grid of 32^3 grid points and a much finer simulation in which we use 96^3 . The latter simulations use the same filter-width $\Delta = L/16$ but correspond to a much higher subgrid resolution $\Delta = 6h_{LES}$. In this way we can clarify some of the dynamics observed on the coarse grid as well as obtain an impression of the actual dynamical consequences associated with the subgrid model.

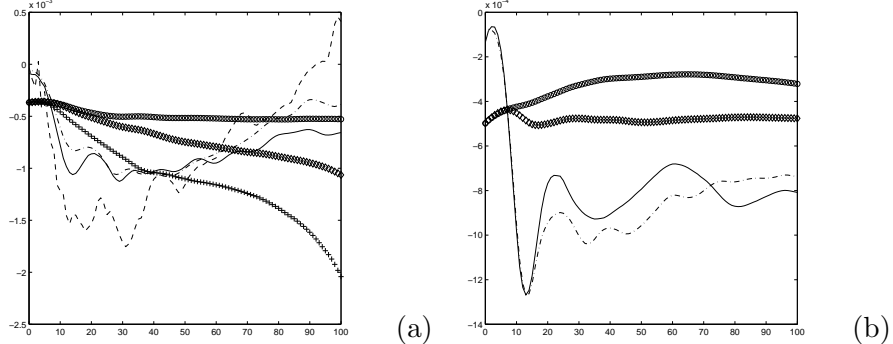


Figure 9. Resolved kinetic energy rate contributions as a function of time: LES- α (dashed line $\partial_t E_m$, +: $\partial_t E_v$), Leray (solid line: $\partial_t E_m$, o: $\partial_t E_v$), filtered nonlinear gradient model (dash-dotted line $\partial_t E_m$, \diamond : $\partial_t E_v$). We used $\kappa = 1$ and show the results for the 32^3 grid in (a) and for the 96^3 grid in (b).

In figure 9 we show the total viscous and subgrid contributions to $\partial_t E$, denoted $\partial_t E_v$ and $\partial_t E_m$, respectively. We notice that on the 32^3 grid the viscous contribution corresponding to the Leray model is quite constant in the turbulent regime and the subgrid contribution gradually becomes of the same order of magnitude. For the filtered nonlinear gradient model we observe a proper dissipation of energy, but slightly less than the Leray model. The corresponding viscous flux contribution increases considerably in the turbulent regime. Finally, for the full LES- α model we observe that the subgrid contribution not only becomes less important in the turbulent regime but even changes sign. This can readily be associated with the overestimated small scale contributions in the solution, as shown in the previous subsection. For the better resolved LES the results of the Leray model and the filtered nonlinear gradient model are quite comparable and appear more predictable. Moreover, all subgrid fluxes are seen to settle and oscillate around some nonzero values, indicating perhaps a more regular self-similar development of the mixing layer in the turbulent regime. The full LES- α model was found to become unstable around $t = 70$, at this high subgrid resolution. Apparently, the explicit filtering, which was found to be essential in the previous section, in order to stabilize the simulation on the coarse grid, is not damping sufficiently well to maintain stability of the LES- α model at increased subgrid resolution.

To further analyse the dynamical behavior, we can look at splitting the subgrid contribution into a positive, i.e., forward scatter or dissipative, contribution and a negative, i.e., backward scatter or reactive

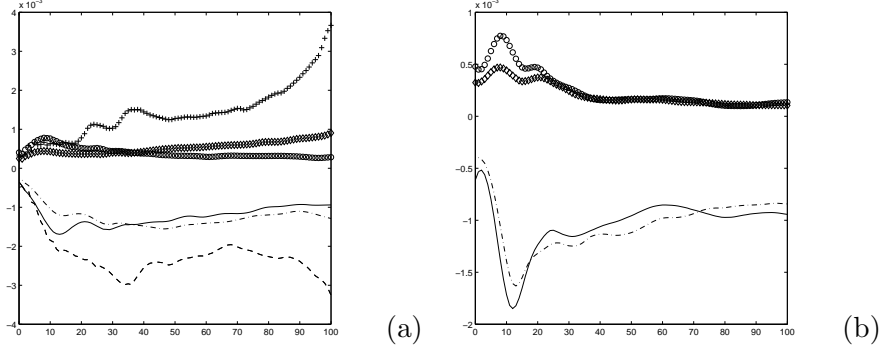


Figure 10. Resolved kinetic energy rate contributions: LES- α (dashed line P_f , +: P_b), Leray (solid line: P_f , o: P_b), filtered nonlinear gradient model (dash-dotted line P_f , \diamond : P_b). We used $\kappa = 1$ and show the results for the 32^3 grid (a) and the 96^3 grid (b).

contribution. To formalize this splitting, we introduce

$$P_b(f) = \int_{\Omega} \frac{1}{2}(f + |f|) \, d\mathbf{x}, \quad P_f(f) = \int_{\Omega} \frac{1}{2}(f - |f|) \, d\mathbf{x} \quad (72)$$

to measure the amount of back-scatter (P_b) and forward scatter of energy (P_f) associated with a term represented by f . In figure 10 we collected the forward and backward scatter contributions for the LES- α models. We observe that all these models predict both forward and backward scatter of energy, which sets them apart from simple eddy-viscosity models that only provide forward scatter. On the coarse grid (32^3) the Leray model and the filtered nonlinear gradient model compare fairly well. The full LES- α model, however, shows a large amount of back-scatter in the turbulent regime and a likewise increased importance of forward scatter. On the finer grid the Leray and filtered nonlinear gradient model show a balance between forward and backward scatter in the turbulent regime.

A third decomposition of the total contribution arises in terms of the individual subgrid-terms. If we consider, e.g., the full LES- α model, written as $m_{ij}^{\alpha} = \overline{A_{ij}} + \overline{B_{ij}} - \overline{C_{ij}}$ we may write

$$\partial_t E = \partial_t E_v + \partial_t E_A + \partial_t E_B - \partial_t E_C \quad (73)$$

with individual contributions due to the viscous fluxes, and the $A-B-C$ terms respectively;

$$\partial_t E_v = \int_{\Omega} -\frac{1}{2Re} \overline{\sigma_{ij}} \overline{\sigma_{ij}} \, d\mathbf{x}, \quad \partial_t E_A = \int_{\Omega} \overline{A_{ij}} \partial_j \overline{u}_i \, d\mathbf{x} \quad (74)$$

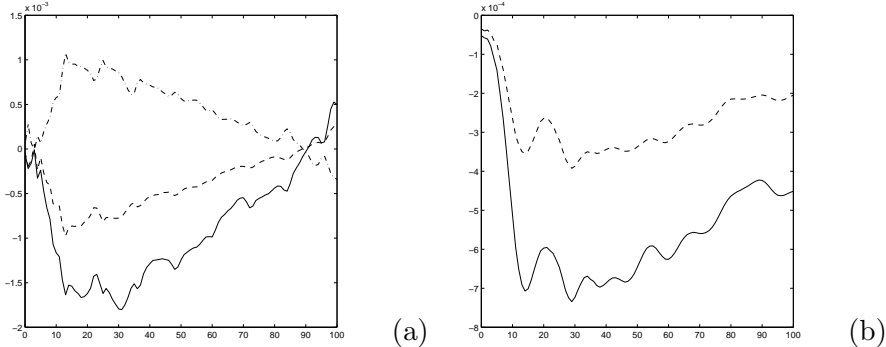


Figure 11. Resolved kinetic energy rate contributions: full LES- α shown in (a) (solid \overline{A} -term, dashed \overline{B} -term, dash-dotted \overline{C} -term), Leray model shown in (b):(solid \overline{A} -term, dashed \overline{B} -term) We used $\kappa = 1$ and show the results for the 32^3 grid.

and similarly for the other terms. In figure 11 we collected the detailed energy-dynamics decomposition corresponding to the two terms which make up the Leray model and the three terms that constitute the full LES- α model. Notice that figure 9 already contains the single contribution of the filtered nonlinear gradient model. The Leray model is seen to be composed of two terms that both dissipate energy. The full LES- α model behaves less regular and we observe that the dissipative \overline{B} contribution is nearly canceled by the reactive \overline{C} contribution.

From this analysis of the resolved energy dynamics it seems that the Leray model and the filtered nonlinear gradient model provide more accurate results and the internal functioning of these models increases the robustness of the model. We also applied the Leray model to a flow at a ten times higher Reynolds number. Although these latter results are still preliminary, it seems that the Leray model provides reliable results, even in such very turbulent flows. Further analysis of this regime is needed though and this will be published elsewhere [37].

In the next section we use the well resolved LES predictions in combination with the coarse grid simulation results to assess the influence of the spatial discretization scheme on the evolution of the flow.

4.3. Toward grid-independent LES- α

The reference simulations considered above, are executed on a fairly coarse grid which corresponds to a ratio between filter-width Δ and grid-spacing h of $\Delta/h = 2$. In many present-day LES, even a ratio of $\Delta/h = 1$ is frequently used. These choices usually arise from considerations of available computational resources, but at the same time imply

that the smallest resolved scales of size on the order of Δ are not accurately represented in the numerical treatment. Hence, there is a strong possibility that the marginal subgrid resolution influences the dynamical properties of the simulated flow.

In order to assess this discretization effect, we will compare the reference LES with simulations at a much higher subgrid resolution. In this way, the effect of subgrid modeling is better represented numerically, while it remains of the same magnitude as in the coarse grid simulation. This allows to isolate the dynamic effects of the spatial discretization in the modeled equations.

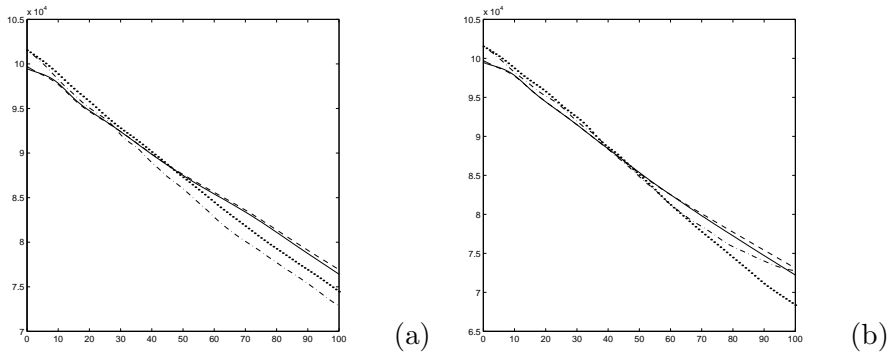


Figure 12. Resolved kinetic energy using the Leray model (a) and the filtered nonlinear gradient model (b): solid line (4th order method, resolution 96^3), dashed line (4th order method, resolution 64^3), dash-dotted line (4th order method, resolution 32^3) and dotted-line (2nd order method, resolution 32^3).

We compare simulations on 32^3 , 64^3 and 96^3 grid-points and focus our attention on the Leray model and the filtered nonlinear gradient model. In figure 12 we compare the predicted resolved kinetic energy obtained with the second and the fourth order accurate spatial discretization method. The subgrid resolution corresponding to these three grids is $\Delta/h = 2$, 4 and 6 respectively. We observe a very close agreement between the predictions using the fourth order accurate method and $\Delta/h = 4$ and 6. This suggests that a mean flow quantity such as the resolved kinetic energy is well represented using $\Delta/h = 4$. Moreover, we notice that on the coarsest grid, the accuracy of the prediction based on the second order method compares closely to that obtained with the fourth order method. Apparently, if the dynamic effects of the spatial discretization errors are quite large, a lower order method can be competitive with a higher order method. For both models the reliability of the predictions on the coarse grid are affected considerably by the coarse-

ness of the subgrid resolution. In both situations, and for both spatial discretizations the effect of the discretization error is seen to enhance the reduction of the resolved kinetic energy.

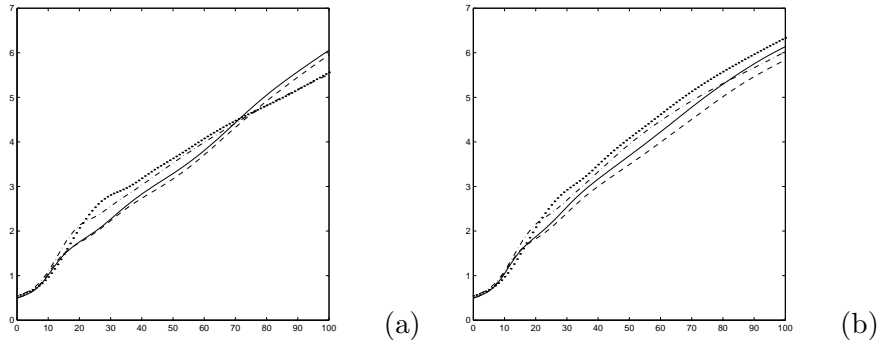


Figure 13. Resolved momentum-thickness using the Leray model (a) and the filtered nonlinear gradient model (b): solid line (4th order method, resolution 96^3), dashed line (4th order method, resolution 64^3), dash-dotted line (4th order method, resolution 32^3) and dotted-line (2nd order method, resolution 32^3).

To further establish the convergence, we show the momentum-thickness in figure 13. We observe that the convergence is clear for the Leray model and that a value of $\Delta/h = 4$ corresponds to reliable predictions for both subgrid models considered, although the sensitivity of the momentum thickness is larger than that of the resolved kinetic energy. Regarding the results for the best resolved simulations, we observe that the momentum-thickness develops very nearly linearly with time in the Leray model, while a slight reduction of the growth-rate predicted by the nonlinear gradient model is seen in the turbulent regime.

Finally, we show the spectra obtained with the Leray and the filtered nonlinear gradient model on the selected grids in figure 14. We notice a general resemblance between the results obtained with both models. As the subgrid resolution is increased, a larger portion of the spectrum is better resolved, cf. the spectra obtained on 64^3 and 96^3 grid-points. Moreover, the differences due to the use of the second order or the fourth order accurate methods are expressed very clearly in the spectra; a strong reduction in energy in the higher wavenumbers on the 32^3 grid results when using the second order method. This is consistent with the stronger attenuation of the high wavenumbers in the second order method, compared to the fourth order accurate method.

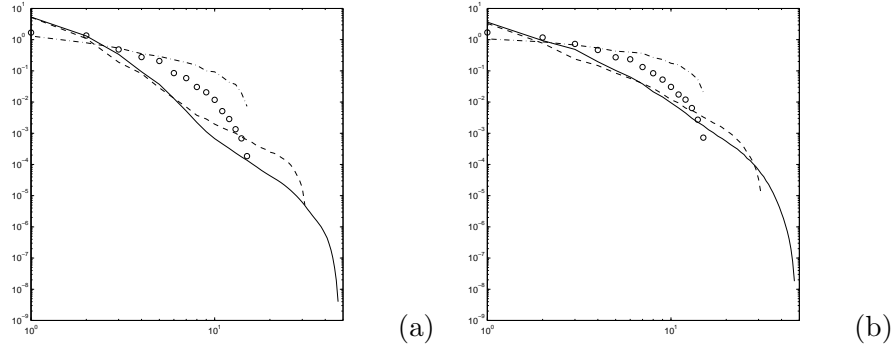


Figure 14. Streamwise kinetic energy spectrum using the Leray model (a) and the filtered nonlinear gradient model (b): solid line (4th order method, resolution 96^3), dashed line (4th order method, resolution 64^3), dash-dotted line (4th order method, resolution 32^3) and marker ‘o’ (2nd order method, resolution 32^3).

5. Concluding remarks

In the α -framework we derived a new subgrid closure for the turbulent stress tensor in LES, by using the Kelvin theorem applied to a filtered transport velocity. The proposed LES- α subgrid model was shown to contain two other subgrid parameterizations, i.e., the nonlinear gradient model and a model corresponding to the Leray regularization of Navier-Stokes dynamics. Moreover, the LES- α model stress tensor contains an explicit filtering in its definition, which sets it apart from other subgrid models in literature. It was shown that this explicit filtering is essential for the LES- α models; without it, the simulations develop a finite time instability. This instability was also observed in an analysis of the viscous one-dimensional Burgers equation and appears to be associated with the nonlinear gradient term.

The flow in a turbulent mixing layer was considered, in order to test the capabilities of the three ‘nested’ LES- α models. Through a comparison with dynamic (mixed) models, we inferred that the Leray model provides particularly accurate predictions. The filtered nonlinear gradient model in turn, compares well with the Leray model and corresponds closely to the Bardina similarity model for the flows considered. The full LES- α model was seen to generate too many small scales in the solution and correspondingly poorer predictions, e.g., too large growth-rate, too high levels of turbulence intensities, etc. An analysis of the resolved kinetic energy dynamics showed that the full LES- α model contains two competing contributions which may tend to cancel and, thus, destabilize some simulations involving this model. In particular, this tendency im-

plied that simulations using the full LES- α model were unstable in our simulations of turbulent mixing at high subgrid resolution.

Apart from accuracy and a certain degree of numerical robustness, the computational overhead associated with a subgrid model is an element of importance in evaluating simulation methods. The computational effort associated with the three LES- α models is considerably lower than that of dynamic (mixed) models. This is primarily a result of the reduction in the number of explicit filtering operations required to evaluate the LES- α model. Moreover, the accuracy of the predictions is higher for the Leray model than for *any* of the other subgrid models considered. Consequently, the Leray model is favored in this study and holds promise for applications to even more complex and demanding flow problems. Preliminary results at significantly higher Reynolds number suggest that the Leray model performs well also in this case.

Finally, we also considered the contribution to the dynamics arising from the spatial discretization method at coarse subgrid resolution. In general, the role of numerical methods in relation to LES has not yet been sufficiently clarified to determine unambiguously whether the accuracy of predictions is restricted because of shortcomings in the subgrid model, or whether this inaccuracy is due to spatial discretization effects. Resolving this ambiguity and determining the main sources of error would help in finding the best strategy for employing computational resources in an LES. In one strategy, a grid-independent solution of the modeled LES equations at fixed filter-width is sought and one only assigns computational resources for reducing numerical errors by increasing the subgrid resolution ratio Δ/h . This approach was applied here and used to evaluate the additional dissipation that arises from the spatial finite volume discretizations at either second order, or fourth order accuracy. This additional dissipation is associated with the implicit filtering effect of the small flow features represented on the grid.

References

- [1] Spalart, P.R.: 1988. Direct simulation of a turbulent boundary layer up to $R_\theta = 1410$. *J. Fluid Mech.* **187**, 61.
- [2] Rogallo, R.S., Moin, P.: 1984. Numerical simulation of turbulent flows. *Ann. Rev. Fluid Mech.* **16**, 99.
- [3] Lesieur, M.: 1990. Turbulence in fluids. *Kluwer Academic Publishers.*, Dordrecht.
- [4] Meneveau, C., Katz, J.: 2000. Scale-invariance and turbulence models for large-eddy simulation. *Ann. Rev. Fluid Mech.* **32**, 1.
- [5] Germano, M.: 1992. Turbulence: the filtering approach. *J. Fluid Mech.* **238**, 325.

- [6] Geurts B.J.: 1999 Balancing errors in LES. Proceedings *Direct and Large-Eddy simulation III: Cambridge*. Eds: Sandham N.D., Voke P.R., Kleiser L., Kluwer Academic Publishers, 1.
- [7] Vreman A.W., Geurts B.J., Kuerten J.G.M.: 1997. Large-eddy simulation of the turbulent mixing layer, *J. Fluid Mech.* **339**, 357.
- [8] Vreman A.W., Geurts B.J., Kuerten J.G.M.: 1994. Realizability conditions for the turbulent stress tensor in large eddy simulation. *J. Fluid Mech.* **278**, 351.
- [9] Ghosal, S.: 1999. Mathematical and physical constraints on large-eddy simulation of turbulence. *AIAA J.* **37**, 425.
- [10] Holm, D.D., Marsden, J.E., Ratiu, T.S.: 1998. Euler-Poincaré equations and semidirect products with applications to continuum theories. *Adv. in Math* **137**, 1.
- [11] Holm, D.D. , Marsden, J.E., Ratiu, T.S.: 1998. Euler-Poincaré models of ideal fluids with nonlinear dispersion. *Phys. Rev. Lett.* **80**, 4173.
- [12] Camassa, R., Holm, D.D.: 1993. An integrable shallow water equation with peaked solitons. *Phys. Rev. Lett.* **71**, 1661.
- [13] Chen, S.Y., Foias, C., Holm, D.D., Olson, E.J., Titi, E.S., Wynne, S.: 1998. The Camassa-Holm equations as a closure model for turbulent channel flow. *Phys. Rev. Lett.* **81**, 5338.
- [14] Chen, S.Y., Foias, C., Holm, D.D., Olson, E.J., Titi, E.S., Wynne, S.: 1999. A connection between Camassa-Holm equations and turbulent flows in channels and pipes. *Phys. Fluids* **11**, 2343.
- [15] Chen, S.Y., Foias, C., Holm, D.D., Olson, E.J., Titi, E.S., Wynne, S.: 1999. The Camassa-Holm equations and turbulence. *Physica D* **133**, 49.
- [16] Chen, S.Y., Holm, D.D., Margolin, L.G., Zhang, R.: 1999. *Direct numerical simulations of the Navier-Stokes alpha model*, *Physica D* **133**, 66.
- [17] Holm, D.D.: 1999. Fluctuation effects on 3D Lagrangian mean and Eulerian mean fluid motion. *Physica D* **133**, 215.
- [18] Marsden, J.E., Shkoller, S.: 2001. The anisotropic Lagrangian averaged Navier-Stokes and Euler equations. *Arch. Ration. Mech. Analysis*. (In the press.)
- [19] Shkoller, S.: 1998. Geometry and curvature of diffeomorphism groups with H^1 metric and mean hydrodynamics. *J. Func. Anal.* **160**, 337.
- [20] Marsden, J.E., Ratiu, T.S., Shkoller, S.: 2000. The geometry and analysis of the averaged Euler equations and a new diffeomorphism group. *Geom. Funct. Anal.* **10**, 582.
- [21] Foias, C., Holm, D.D., Titi, E.S.: 2002. The three dimensional viscous Camassa-Holm equations, and their relation to the Navier-Stokes equations and turbulence theory. *J. Diff. Eqs.* to appear.
- [22] Marsden, J.E., Shkoller, S.: 2001. Global well-posedness for the Lagrangian averaged Navier-Stokes (LANS- α) equations on bounded domains. *Phil. Trans. R. Soc. Lond. A* **359**, 1449.
- [23] Foias, C., Holm, D.D., Titi, E.S.: 2001. The Navier-Stokes-alpha model of fluid turbulence. *Physica D* **152** 505.
- [24] Domaradzki, J.A., Holm, D.D.: 2001. Navier-Stokes-alpha model: LES equations with nonlinear dispersion. *Modern simulation strategies for turbulent flow*. Edwards Publishing, Ed. B.J. Geurts. 107.

- [25] Mohseni, K., Kosovic, B., Marsden, J.E., Shkoller, S., Carati, D., Wray, A., Rogallo, R.: 2000. Numerical simulations of homogeneous turbulence using the Lagrangian averaged Navier-Stokes equations. *Proc. of the 2000 Summer Program*, 271. Stanford, CA: NASA Ames / Stanford University.
- [26] Holm, D.D., Kerr, R.: 2001. Transient vortex events in the initial value problem for turbulence. In preparation.
- [27] Holm, D.D.: 1999. Alpha models for 3D Eulerian mean fluid circulation. *Nuovo Cimento C* **22**, 857.
- [28] Bardina, J., Ferziger, J.H., Reynolds, W.C.: 1983. Improved turbulence models based on large eddy simulations of homogeneous incompressible turbulence. Stanford University, Report TF-19.
- [29] Leonard, A.: 1974. Energy cascade in large-eddy simulations of turbulent fluid flows. *Adv. Geophys.* **18**, 237.
- [30] Clark, R.A., Ferziger, J.H., Reynolds, W.C.: 1979. Evaluation of subgrid-scale models using an accurately simulated turbulent flow. *J. Fluid Mech.* **91**, 1.
- [31] Vreman A.W., Geurts B.J., Kuerten J.G.M.: 1996. Large eddy simulation of the temporal mixing layer using the Clark model *TCFD8*, 309.
- [32] Winckelmans, G.S., Jeanmart, H., Wray, A.A., Carati, D., Geurts, B.J.: 2001. Tensor-diffusivity mixed model: balancing reconstruction and truncation. *Modern simulation strategies for turbulent flow*. Edwards Publishing, Ed. B.J. Geurts. 85.
- [33] Leray, J.: 1934. Sur le mouvement d'un liquide visqueux emplissant l'espace *Acta Math.* **63**, 193.
- [34] Vreman A.W., Geurts B.J., Kuerten J.G.M.: 1995. A priori tests of Large Eddy Simulation of the compressible plane mixing layer. *J. Eng. Math.* **29**, 299
- [35] de Bruin, I.C.C.: 2001. Direct and large-eddy simulation of the spatial turbulent mixing layer. *Ph.D. Thesis*, Twente University Press.
- [36] Germano, M., Piomelli U., Moin P., Cabot W.H.: 1991. A dynamic subgrid-scale eddy viscosity model. *Phys.of Fluids* **3**, 1760
- [37] Geurts, B.J., Holm, D.D.: 2001. Leray simulation of turbulent flow. In preparation.
- [38] Ghosal, S.: 1996. An analysis of numerical errors in large-eddy simulations of turbulence. *J. Comp. Phys.* **125**, 187.
- [39] Vreman A.W., Geurts B.J., Kuerten J.G.M.: 1996. Comparison of numerical schemes in Large Eddy Simulation of the temporal mixing layer. *Int.J.Num. Meth. in Fluids* **22**, 297.
- [40] Vreman A.W., Geurts B.J., Kuerten J.G.M.: 1994. Discretization error dominance over subgrid-terms in large eddy simulations of compressible shear layers. *Comm.Num.Meth.Eng.Math.* **10**, 785.
- [41] Geurts, B.J., Fröhlich, J.: 2001. Numerical effects contaminating LES: a mixed story. *Modern simulation strategies for turbulent flow*. Edwards Publishing, Ed. B.J. Geurts. 309.
- [42] Geurts B.J., Vreman A.W., Kuerten J.G.M.: 1994. Comparison of DNS and LES of transitional and turbulent compressible flow: flat plate and mixing layer. *Proceedings 74th Fluid Dynamics Panel and Symposium on Application of DNS and LES to transition and turbulence, Crete*, AGARD Conf. Proceedings 551:51

- [43] Ghosal, S., Moin, P.: 1995. The basic equations for large-eddy simulation of turbulent flows in complex geometry. *J. Comp. Phys.* **286**, 229.
- [44] Du Vachat, R.: 1977. Realizability inequalities in turbulent flows. *Phys. Fluids* **20**, 551.
- [45] Schumann, U.: 1977. Realizability of Reynolds-stress turbulence models. *Phys. Fluids* **20**, 721.
- [46] Ortega, J.M.: 1987. Matrix Theory. *Plenum Press*. New York
- [47] Ghosal, S., Lund, T.S., Moin, P., Akselvoll, K.: 1995. A dynamic localization model for large-eddy simulation of turbulent flows. *J. Fluid Mech.* **286**, 229.
- [48] Lilly, D.K.: 1992. A proposed modification of the Germano subgrid-scale closure method. *Phys. of Fluids A* **4**, 633.
- [49] Geurts, B.J.: 1997. Inverse modeling for large-eddy simulation. *Phys. of Fluids* **9**, 3585.
- [50] Kuerten J.G.M., Geurts B.J., Vreman, A.W., Germano, M.: 1999. Dynamic inverse modeling and its testing in large-eddy simulations of the mixing layer. *Phys. Fluids* **11**, 3778.
- [51] Horiuti, K.: Constraints on the subgrid-scale models in a frame of reference undergoing rotation. *J. Fluid Mech.*, submitted.
- [52] Germano, M.: 1986. Differential filters for the large eddy numerical simulation of turbulent flows. *Phys Fluids* **29**, 1755.
- [53] Smagorinsky, J.: 1963. General circulation experiments with the primitive equations. *Mon. Weather Rev.* **91**, 99.
- [54] Stolz, S., Adams, N.A.: 1999. An approximate deconvolution procedure for large-eddy simulation. *Phys. of Fluids*, **11**, 1699.
- [55] Domaradzki, J.A., Saiki, E.M.: 1997. A subgrid-scale model based on the estimation of unresolved scales of turbulence. *Phys. of Fluids* **9**, 1.
- [56] Wasistho, B., Geurts, B.J., Kuerten, J.G.M.: 1997. Numerical simulation of separated boundary layer flow. *J. Engg. Math* **32**, 179.
- [57] Chatelin, F.: 1993. Eigenvalues of matrices. *John Wiley & Sons*. Chichester.
- [58] Jameson, A.: 1983. Transonic flow calculations. *MAE-Report 1651*, Princeton
- [59] Geurts, B.J., Kuerten, J.G.M.: 1993. Numerical aspects of a block-structured flow solver. *J. Engg. Math.* **27**, 293.